

NON-DOUBLE-COUPLE EARTHQUAKES

1. THEORY

Bruce R. Julian
U.S. Geological Survey
Menlo Park, California

Angus D. Miller¹ and G. R. Foulger¹
Department of Geological Sciences
University of Durham
Durham, England, United Kingdom

Abstract. Historically, most quantitative seismological analyses have been based on the assumption that earthquakes are caused by shear faulting, for which the equivalent force system in an isotropic medium is a pair of force couples with no net torque (a “double couple,” or DC). Observations of increasing quality and coverage, however, now resolve departures from the DC model for many earthquakes and find some earthquakes, especially in volcanic and geothermal areas, that have strongly non-DC mechanisms. Understanding non-DC earthquakes is important both for studying the process of faulting in detail and for identifying nonshear-faulting processes that apparently occur in some earthquakes. This paper summarizes the theory of “moment tensor” expansions of equivalent-force systems and analyzes many possible physical non-DC earthquake processes. Contrary to long-standing assumption, sources within

the Earth can sometimes have net force and torque components, described by first-rank and asymmetric second-rank moment tensors, which must be included in analyses of landslides and some volcanic phenomena. Non-DC processes that lead to conventional (symmetric second-rank) moment tensors include geometrically complex shear faulting, tensile faulting, shear faulting in an anisotropic medium, shear faulting in a heterogeneous region (e.g., near an interface), and polymorphic phase transformations. Undoubtedly, many non-DC earthquake processes remain to be discovered. Progress will be facilitated by experimental studies that use wave amplitudes, amplitude ratios, and complete waveforms in addition to wave polarities and thus avoid arbitrary assumptions such as the absence of volume changes or the temporal similarity of different moment tensor components.

1. INTRODUCTION

Most earthquakes are caused by shear faulting. The recognition of this fact [Gilbert, 1884; Lawson, 1908; Reid, 1910] marked the beginning of seismology as a science, although for several decades, mathematical theory was inadequate to predict the static and dynamic displacement fields of faults or other hypothetical physical sources. Seismologists debated in particular whether a shear fault is equivalent to a force couple, as seems intuitive, or to a pair of couples whose torques cancel each other (a “double couple,” or DC). Single-couple sources were originally supposed to model faulting, and DCs were used to represent the sudden vanishing of shear strength [Aki, 1979]. Single-couple theories continued to be applied to faulting until Maruyama [1963], and independently Burridge and Knopoff [1964], rigorously established that a shear fault in an isotropic elastic medium is equivalent to a distribution of DCs over the fault surface.

Figure 1 illustrates the relationship between a shear

fault and the equivalent distribution of DC force systems. It also shows the radiation patterns of seismic body waves from a single DC, to which a fault is equivalent in the point source (long wavelength) approximation. For compressional waves, this pattern consists of four symmetrical lobes of alternating polarity. Compressional wave amplitudes vanish in the fault plane and also in an “auxiliary plane” perpendicular to it. The shear wave radiation pattern is also symmetric with respect to these two planes, as are the entire static and dynamic displacement fields, so the fault plane cannot be identified from seismic or geodetic data in the point source approximation.

During the early years of seismology, some theories attributed earthquakes to processes other than shear faulting. Ishimoto [1932] in particular, thought that earthquakes resulted from subterranean magma motion, and modeled this process using force systems that produce conical, rather than planar, nodal surfaces for compressional waves. In recent decades, however, the model of an earthquake as a DC force system has underlain most quantitative analysis of seismic waves and has been highly successful in enabling seismologists to use earthquakes to advance our understanding of tectonic processes [e.g., Sykes, 1967; Isacks *et al.*, 1968].

¹Also at U.S. Geological Survey, Menlo Park, California.

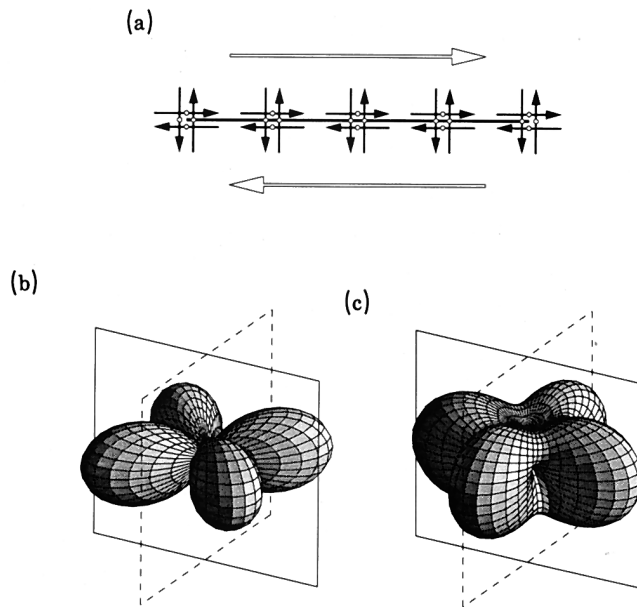


Figure 1. The double-couple earthquake source mechanism. (a) Plan view of a vertical strike-slip shear fault in an isotropic medium, showing the direction of slip (open arrows), and the equivalent distribution of double-couple force systems (solid arrows, with forces applied at white dots). (b) Radiation pattern of compressional waves, showing fault plane (solid lines), and auxiliary plane (dashed lines). Adjacent lobes have opposite polarity. (c) Same as Figure 1b, but for shear waves. These radiation patterns are normalized with respect to their maximum values. For true comparison, the shear wave pattern should be enlarged by a factor of $(V_P/V_S)^3$ ($3^{3/2} \approx 5.2$, for a Poisson solid.) The shear wave polarization direction is the transverse component of the gradient of the compressional wave amplitude.

As seismological instrumentation and analysis methods improved, however, departures from the idealized DC theory were observed. A growing number of earthquakes are found to have anomalous mechanisms inconsistent with shear faulting. These earthquakes range in size over many orders of magnitude and occur in many geological environments, although they are most common in volcanic and geothermal areas. The physical causes of these earthquakes are not yet well understood, and it is likely that more than one process is involved.

At the same time, small departures from the DC model are found for nearly all earthquakes studied routinely using high-quality data from global digital seismograph networks. Most of these non-DC components are probably artifacts of noisy data or imperfect modeling methods, but many of them are well resolved. These must indicate departures from idealized fault models, such as curvature of faults or components of motion normal to fault surfaces. Further advances in high-resolution studies of earthquake mechanisms, and of non-DC components in particular, can be expected to play an important role in elucidating the roles of factors such as geometrical fault complexity, tensile failure, dilatancy, and fluid flow in faulting.

A prerequisite for studying non-DC earthquake mechanisms effectively is a mathematical method for describing them. This is provided by the “moment tensor” [Gilbert, 1970], a generalized source representation that encompasses DCs, more general types of shear forces, and volumetric forces. The moment tensor also has important computational properties. In particular, it yields linear mathematical expressions for displacement fields, which facilitate their computation and enormously simplify the inverse problem of deducing source mechanisms from observations.

Studying non-DC components of earthquakes provides an opportunity to obtain new information about Earth processes. In the case of volcanic and geothermal earthquakes, this information may facilitate the exploitation of geothermal energy and help in predicting volcanic activity. Deep earthquakes have been regarded as paradoxical since they were first discovered, and their causes are still not well understood. Many proposed deep-earthquake processes involve polymorphic phase transitions and volume changes, so non-DC earthquake mechanisms are central to testing such theories.

This paper summarizes seismic source theory and describes possible physical processes that are candidates for causing non-DC earthquakes. A companion paper [Miller *et al.*, this issue] describes observations of such events, using the material in this paper as a foundation.

2. QUANTITATIVE DESCRIPTION OF EARTHQUAKE MECHANISMS

2.1. Introduction

It is conventional to represent an earthquake mathematically by a system of equivalent forces. For a shear fault in an isotropic elastic medium, this force system is a DC. In order to investigate possible causes of non-DC earthquakes, we first outline the theory that connects physical earthquake processes with equivalent force systems.

2.2. Equivalent Force System

2.2.1. Failure processes. Physically, an earthquake involves some kind of nonlinear failure process, such as fracture or frictional sliding, acting within a limited region. The equivalent force system, acting in an intact (unfaulted) “model” medium, would produce the same displacement field outside the source region. The model medium is chosen to be mathematically tractable and usually is linearly elastic, isotropic, and spatially homogeneous. Any physical source has a unique equivalent force system in a given model medium, but the converse statement is not true. Many different physical processes can have identical force systems and therefore identical static and dynamic displacement fields.

Because the equivalent force system is all that can be deduced from observations of displacement fields, it

constitutes a kind of phenomenological description of the source. There is a one-to-one correspondence between equivalent force systems and elastodynamic fields outside the source region, so we can, in principle at least, determine force systems from observations. On the other hand, the correspondence between force systems and physical source processes is one-to-many, so equivalent force systems (and therefore seismic and geodetic observations) cannot uniquely diagnose physical source processes. A familiar example of this nonuniqueness is the ambiguity between a fault plane and the “auxiliary plane” orthogonal to it. Faulting on either of these planes produces identical long-wavelength radiation (section 2.4.2).

The failure process can be regarded as a sudden localized change in the constitutive relation (stress-strain law) in the Earth [Backus and Mulcahy, 1976a, b]. Before an earthquake the stress field satisfies the equations of equilibrium. At the time of failure, a rapid change in the constitutive relation causes the stress field to change. The resulting disequilibrium causes dynamic motions that radiate elastic waves. For illustrative purposes, we disregard the effect of gravity in the following discussion. In the absence of external forces, the equation of motion is

$$\rho \ddot{u}_i = \sigma_{ij,j} \quad (1)$$

where $\rho(\mathbf{x})$ is density, $\mathbf{u}(\mathbf{x}, t)$ is the particle displacement vector, $\boldsymbol{\sigma}(\mathbf{x}, t)$ is the physical stress tensor, \mathbf{x} is position, and t is time. Dots indicate differentiation with respect to t , ordinary subscripts indicate Cartesian components of vectors or tensors, the subscript “ j ” indicates differentiation with respect to the j th Cartesian spatial coordinate x_j , and duplicated indices indicate summation. The true stress is unknown, however, so in theoretical calculations we use the stress $\mathbf{s}(\mathbf{x}, t)$, given by the constitutive law of the model medium (usually Hooke’s law). If we replace σ_{ij} by s_{ij} in the equations of motion, though, we must also introduce a correction term, $\mathbf{f}(\mathbf{x}, t)$:

$$\rho \ddot{u}_i = s_{ij,j} + f_i, \quad (2)$$

$$f_i \stackrel{\text{def}}{=} (\sigma_{ij} - s_{ij}),_j. \quad (3)$$

This term has the form of a body-force density, and is the equivalent force system of the earthquake. It differs from zero only within the source region. The difference between the true physical stress and the model stress, appearing in parentheses on the right side of (3), has been termed the “stress glut” by Backus and Mulcahy [1976a, b].

2.2.2. Net forces and torques. Since the 1960s, when single-couple force systems were shown to be inappropriate models of shear faults, nearly all analyses of earthquake source mechanisms have explicitly excluded net forces and torques from consideration. The equivalent forces given by (3), which arise from the imbalance between true physical stresses and those in

the model, are consistent with these restrictions. Because the stress glut $\sigma_{ij} - s_{ij}$ is symmetric, \mathbf{f} exerts no net torque at any point. Furthermore, because $\sigma_{ij} - s_{ij}$ vanishes outside the source region, Gauss’ theorem implies that the total force exerted vanishes at each instant.

More complete analysis, however, including the effects of gravitation and mass advection, shows that equation (3) is based on overly restrictive assumptions and that net force and torque components are possible for realistic sources within the Earth [Takei and Kumazawa, 1994]. Additional forces arise from (1) differences between the Earth’s true density distribution and that in the model, (2) time variations in density caused by mass advection, (3) differences between true particle acceleration and that obtained by linearizing the Eulerian description of motion, (4) differences between the true gravitational acceleration and that in the model, and (5) variations in gravity caused by the mass variations (effects 1 and 2). The unbalanced forces and torques arising from these effects transfer linear and angular momentum between the source region and the rest of the Earth, with both types of momentum conserved for the entire Earth. An easily understood example is the collapse of a cavity, in which rocks fall from the ceiling to the floor. While the rocks are falling, the Earth outside the cavity experiences a net upward force, relative to the state before and after the event.

The net force component in any source is constrained by the principle of conservation of momentum; because the source region is at rest before and after the earthquake, the total impulse of the equivalent force (its time integral) must vanish. Surprisingly, no such requirement holds for the torque. The total torque exerted by gravitational forces need not vanish even after the earthquake. Horizontal displacement of the center of mass of the source region leads to a gravitational torque, which must be balanced by stresses on the boundary of the source and causes the radiation of elastic waves. Because gravity acts vertically, there can be no net torque about a vertical axis.

We cannot use the equivalent force system $\mathbf{f}(\mathbf{x}, t)$ and the elastodynamic equation (2) to determine the displacement field for a hypothetical source process. The equivalent force system itself depends on the displacement field that is being sought. Two different approaches are commonly used:

1. In the kinematic approach we assume some mathematically tractable displacement field in the source region (e.g., suddenly imposed slip, constant over a rectangular fault plane), derive the equivalent force system from equation (3), and solve (2) for the resulting displacement field outside the source region [e.g., Haskell, 1964; Savage, 1966; Okada, 1985, 1992].

2. In the inverse approach we use (2) to determine the force system $\mathbf{f}(\mathbf{x}, t)$ from the observed displacement field, and compare the result with force systems predicted theoretically for hypothesized source processes.

The most useful way to parameterize the force system in this approach is to use its spatial moments.

2.3. Moment Tensor

2.3.1. Moment tensor expansion for the response.

Given the equivalent force system $\mathbf{f}(\mathbf{x}, t)$, computing the response of the Earth is a linear problem, and its solution can be expressed as an integral over the source region V [Aki and Richards, 1980, equation 3.1] (omitting displacement and traction discontinuities for simplicity):

$$u_i(\mathbf{x}, t) = \iiint_V G_{ij}(\mathbf{x}, \boldsymbol{\xi}, t) * f_j(\boldsymbol{\xi}, t) d^3\xi, \quad (4)$$

where $G_{ij}(\mathbf{x}, \boldsymbol{\xi}, t)$ is the Green's function, which gives the i th component of displacement at position \mathbf{x} and time t caused by an impulsive force in the j direction applied at position $\boldsymbol{\xi}$ and time 0, and the asterisk indicates temporal convolution. If we expand the Green's function in a Taylor series in the source position $\boldsymbol{\xi}$,

$$G_{ij}(\mathbf{x}, \boldsymbol{\xi}, t) = G_{ij}(\mathbf{x}, \mathbf{0}, t) + G_{ij,k}(\mathbf{x}, \mathbf{0}, t)\xi_k + \cdots, \quad (5)$$

equation (4) for the response becomes

$$u_i(\mathbf{x}, t) = G_{ij}(\mathbf{x}, \mathbf{0}, t) * F_j(t) + G_{ij,k}(\mathbf{x}, \mathbf{0}, t) * M_{jk}(t) + \cdots, \quad (6)$$

where

$$F_j(t) \stackrel{\text{def}}{=} \iiint_V f_j(\boldsymbol{\xi}, t) d^3\xi \quad (7)$$

is the total force exerted by the source and

$$M_{jk}(t) \stackrel{\text{def}}{=} \iiint_V \xi_k f_j(\boldsymbol{\xi}, t) d^3\xi \quad (8)$$

is the moment tensor. If the equivalent force is derivable from a stress glut via (3), then it can be shown that the moment tensor is the negative of the volume integral of the stress glut:

$$M_{jk}(t) = - \iiint_V (\sigma_{ij} - s_{ij}) d^3\xi \quad (9)$$

The moment tensor is a second-rank tensor, which describes a superposition of nine elementary force systems, with each component of the tensor giving the strength (moment) of one force system. The diagonal components M_{11} , M_{22} , and M_{33} correspond to linear dipoles that exert no torque, and the off-diagonal elements M_{12} , M_{13} , M_{21} , M_{23} , M_{31} , and M_{32} correspond to force couples. It is usually assumed that the moment tensor is symmetric ($M_{12} = M_{21}$, $M_{13} = M_{31}$, $M_{23} = M_{32}$), so that the force couples exert no net torque (see above), in which case only six moment tensor compo-

nents are independent. In this case, the off-diagonal components correspond to three pairs of force couples, each exerting no net torque ("double couples").

The magnitudes of the six (or nine) elementary force systems (the moment tensor components) transform according to standard tensor laws under rotations of the coordinate system, so there exist many different combinations of elementary forces that are equivalent. In particular, for a symmetric, six-element moment tensor one can always choose a coordinate system in which the force system consists of three orthogonal linear dipoles, so that the moment tensor is diagonal. In other words, a general point source can be described by three values (the principal moments) that describe its physics and three values that specify its orientation.

The moment tensor has three important properties that make it useful for representing seismic sources. (1) It makes the "forward problem" of computing theoretical seismic-wave excitation linear. A general source is represented as a weighted sum of elementary force systems, so any seismic wave is just the same weighted sum of the waves excited by the elementary sources. The linearity of the forward problem in turn makes much more tractable the inverse problem of determining source mechanisms from observations. (2) It simplifies the computation of wave excitation. By transforming the moment tensor into an appropriately oriented coordinate system, the angles defining the observation direction can be made to take on special values such as 0 and $\pi/2$. Thus radiation by the elementary sources must be computed not for a general direction, but for only a few directions for which the computation is easier. In a laterally homogeneous medium, for example, radiation must be computed for only a single azimuth. (3) The moment tensor is more general than the DC representation. It includes DCs as special cases but has two more free parameters than a DC (six versus four), which enable it to represent sources involving volume changes and more general types of shear than simple slip on a plane. It is this generality that makes the moment tensor representation important in studying non-DC earthquakes.

2.3.2. Higher-rank moment tensors. As equation (6) shows, "the" moment tensor described above is only one of an infinite sequence of spatial moments that appear in the expansion of the Earth's response to an earthquake. The later terms involve higher-rank moment tensors, which contain information about the spatial and temporal distribution of failure in an earthquake, and have great potential value for studying source finiteness and rupture propagation [Stump and Johnson, 1982]. Both the total force defined in equation (7) and the moment tensor defined in (8) may be regarded as special cases of the general spatial moment

$$M_{jkl \dots}(t) \stackrel{\text{def}}{=} \iiint_V \xi_k \xi_l \cdots f_j(\boldsymbol{\xi}, t) d^3\xi, \quad (10)$$

of order s (i.e., having s spatial indices $k, l \dots$). Because the arrangement of the spatial indices is irrelevant, the number of independent components is three (the number of components of the force \mathbf{f}) times the number of possible products $\xi_k \xi_l \dots$ (the number of selections of three things taken s at a time with duplications allowed), or in total, $3 \binom{s+2}{2}$. Thus the total force ($s = 0$) has 3 components, the first-order (second rank) moment tensor ($s = 1$) has 9 components, and the second-order (third rank) moment tensor has 18 components. (The larger numbers given by *Stump and Johnson* [1982, p. 725] fail to take into account the symmetry with respect to permutation of the spatial indices implied by the definition (10).)

Instead of regarding the spatial moments as functions of time, we can describe the time-dependence of the source using spatiotemporal moments,

$$M_{jkl}^{(q)} \stackrel{\text{def}}{=} \int dt \iiint_V t^q \xi_k \xi_l \dots \dot{f}_j(\xi, t) d^3\xi. \quad (11)$$

It is necessary to use the time derivative of the equivalent force, \dot{f} , here, because for most seismic sources f approaches a nonzero value as $t \rightarrow \infty$ [*Backus and Mulcahy* [1976a, section 7]]. Reasoning as above, we find that the number of independent components is $3 \binom{s+q+3}{3}$.

Because higher-rank moment tensors have so many components, few attempts have yet been made to determine them from observed seismic waves. Such work is sure to play an increasingly important role in future studies of earthquake processes, especially those of non-DC earthquakes, because higher moments describe the orientation and geometry of the failure zone, whereas first moments (conventional second-rank moment tensors) do not.

2.3.3. Moment centroid. Representing an earthquake as a point source raises the question of where this point is located, or equivalently, where the origin of the coordinate system is to be taken in the definitions (10) and (11). From the definition (7), it is clear that the total force \mathbf{F} does not depend on the origin, and furthermore, from definition (8), if the total force vanishes, then the conventional second-rank moment tensor also is independent of the origin. (Experimentally determined moment tensors, however, can depend on the origin because the Green's functions depend on the assumed source position.) The higher moments, however, do depend on the origin, and we can use this fact to choose the origin objectively.

For nonnegative scalar distributions such as mass and probability density, the centroid of the distribution is for most purposes the “best point source” location. The centroid has the properties of (1) having vanishing first moments and (2) minimizing the second moments (moments of inertia, in the case of mass, or variances, in the case of probability), which measure the spreads of the

distributions about the chosen point. It is not straightforward to extend these concepts to elastodynamics, however. The equivalent force $\mathbf{f}(\mathbf{x}, t)$ is a vector distribution, so it has three centroids, and furthermore if the total force \mathbf{F} defined in (7) vanishes (as is usually assumed), then the centroidal coordinates are undefined. *Backus* [1977] suggested defining the centroid as the point that minimizes in a least-squares sense the second moments. The centroid as thus defined minimizes $\sum_{ijk} (M_{ijk}^{(0)})^2$ with respect to the three spatial coordinates of the centroid and minimizes $\sum_{ij} (M_{ij}^{(1)})^2$ with respect to the temporal centroid. This definition is used in “centroid moment tensor” analyses, such as those conducted regularly in nearly real time by Harvard University [*Dziwiewonski et al.*, 1981] and the Earthquake Research Institute of Tokyo University [*Kawakatsu et al.*, 1994] (section 3.5.3 below).

The centroid of moment release is not the same as the hypocenter of an earthquake, which is the location usually reported in seismological bulletins. The hypocenter is the point of origin of the first-arriving seismic waves, the point at which rapid failure begins in an earthquake. The centroid locates the dominant moment release and represents better the entire earthquake, rather than only its beginning.

2.4. Surface Sources (Faults)

2.4.1. Basic principles. A fault is a surface across which there is a discontinuity in displacement. The equivalent force distribution \mathbf{f} for a generally oriented fault in an elastic medium can be deduced from (2), if we use generalized functions (the Dirac delta function and its derivatives) to represent quantities on the fault surface. The general result is

$$f_k(\boldsymbol{\eta}, t) = - \iint_A [u_i(\boldsymbol{\xi}, t)] c_{ijkl} v_j \frac{\partial}{\partial \eta_l} \delta(\boldsymbol{\eta} - \boldsymbol{\xi}) dA, \quad (12)$$

where $\boldsymbol{\eta}$ is the position where the force is evaluated, $\boldsymbol{\xi}$ is the position of the element of area dA , and the integration extends over the fault surface [*Aki and Richards*, 1980, equation 3.5]. The unit vector normal to the fault surface is $\mathbf{v}(\boldsymbol{\xi})$, and $[\mathbf{u}(\boldsymbol{\xi}, t)]$ is the displacement discontinuity across the fault in the direction of \mathbf{v} . The components of the elastic modulus tensor are c_{ijkl} , and $\delta(\mathbf{x})$ is the three-dimensional Dirac delta function.

Substituting the force distribution from equation (12) into (8), we get the moment tensor of a general fault,

$$M_{ij} = -c_{ijkl} A \overline{v_k [u_l]}, \quad (13)$$

where A is the total fault area and the overbar indicates the average value over the fault.

Two important special cases, shear faults and tensile faults, illustrate the use of (13).

2.4.2. Shear faults. For a planar shear fault (with normal \mathbf{v} in the x_3 direction and displacement disconti-

nuity $[\mathbf{u}]$ in the x_1 direction, say, so that $v_1 = v_2 = 0$ and $[u_2] = [u_3] = 0$ in a homogeneous isotropic medium ($c_{ijkl} = \lambda \delta_{ij} \delta_{km} \delta_{lm} + 2\mu \delta_{ik} \delta_{jl}$, so $\sigma_{ij} = \lambda \delta_{ij} e_{mm} + 2\mu e_{ij}$, where e_{ij} are the components of the strain tensor, λ and μ are the Lamé elastic moduli, and δ_{ij} is the Kronecker delta tensor), equation (8) gives a moment tensor with a single pair of nonzero components $M_{13} = M_{31} = \mu A \bar{u}$, where \bar{u} is the average slip. This corresponds to a pair of force couples, one with forces in the x_1 direction and moment arm in the x_3 direction, and the other with these directions interchanged.

For idealized faulting sources, with nonlinear effects restricted to a mathematical surface, the source region has no mass or moment of inertia and cannot exchange linear or angular momentum with the rest of the Earth. Therefore the assumptions of vanishing net force and torque are justified for such faulting sources.

Note that we get the same DC moment tensor for a fault with normal in the x_1 direction and displacement discontinuity in the x_3 direction. This ambiguity between “conjugate” faults is a familiar example of the fundamental limitations on the information that can be deduced from equivalent force systems.

2.4.3. Tensile faults. Another important special case is a planar tensile fault in an isotropic medium. If the fault lies in the x_1 - x_2 plane and opens in the x_3 direction, then $v_1 = v_2 = 0$ and $[u_1] = [u_2] = 0$. Equation (8) gives a moment tensor with three nonzero components: $M_{11} = M_{22} = \lambda A \bar{u}$ and $M_{33} = (\lambda + 2\mu) A \bar{u}$. This corresponds to three orthogonal dipoles. Two dipoles lie in the fault plane and have moments of $\lambda A \bar{u}$, and the third is normal to the fault and has a moment of $(\lambda + 2\mu) A \bar{u}$.

2.5. Three-Dimensional Sources

Some possible non-DC source processes, such as polymorphic phase transformation, occur throughout a finite volume rather than on a surface. The equivalent force system for many such volume sources can be expressed in terms of the “stress-free strain,” Δe_{ij} [Eshelby, 1957], which is the strain that would occur in the source region if the tractions on its boundary were held constant by externally applied artificial forces. By reasoning that involves a sequence of imaginary cutting, straining, and welding operations [e.g., Aki and Richards, 1980, section 3.4], the moment tensor of a volume source is found to be

$$M_{ij} = \iiint_V c_{ijkl} \Delta e_{kl} dV. \quad (14)$$

For an isotropic volume change of ΔV in an isotropic medium, for example,

$$M_{ij} = (3\lambda + 2\mu) \Delta V \delta_{ij}. \quad (15)$$

2.6. Decomposing Moment Tensors

The description of an earthquake source in terms of moment tensor components is not well suited to human

comprehension. To make a moment tensor easier to understand, it helps to decompose it into elementary force systems. First, we express the moment tensor in its principal axis coordinate system. Three values (the Euler angles, for example) are required to specify the orientation of this system, and three other values specify the moments of three orthogonal dipoles oriented parallel to the coordinate axes. Writing these three principal moments as a column vector, we first decompose the moment tensor into an isotropic force system and a deviatoric remainder,

$$\begin{bmatrix} M_1 \\ M_2 \\ M_3 \end{bmatrix} = M^{(V)} \begin{bmatrix} 1 \\ 1 \\ 1 \end{bmatrix} + \begin{bmatrix} M'_1 \\ M'_2 \\ M'_3 \end{bmatrix}, \quad (16)$$

with $M^{(V)} = (M_1 + M_2 + M_3)/3$, and then we decompose the deviatoric part into a DC (principal moments in the ratio 1:−1:0) and a “compensated linear vector dipole” (CLVD), which is a source with principal moments in the ratio 1:−1/2:−1/2 [Knopoff and Randall, 1970]. Figure 2 illustrates the three elementary force systems used in this decomposition, showing their compressional wave radiation patterns and the distributions of compressional wave polarities on the focal sphere (an imaginary sphere surrounding the earthquake hypocenter, to which observations are often referred). Many other decompositions of the deviatoric part are possible, including many decompositions into two DCs, or into two CLVDs. Figure 3 illustrates several possibilities taken from the seismological literature. The question of how to decompose the deviatoric part of a moment tensor is surprisingly troublesome. Many schemes in common use, including the one illustrated in Figure 3e, which is used in routinely produced moment tensor catalogs (section 3.5.3), have undesirable properties, such as changing pure DC or CLVD mechanisms into mixed mechanisms. The method of Knopoff and Randall [1970] (Figure 3f), which makes the major axis of the CLVD coincide with the corresponding axis of the DC, avoids such pathological behavior and is the method most widely used in seismological research:

$$\begin{bmatrix} M'_1 \\ M'_2 \\ M'_3 \end{bmatrix} = M^{(\text{DC})} \begin{bmatrix} 0 \\ -1 \\ 1 \end{bmatrix} + M^{(\text{CLVD})} \begin{bmatrix} -\frac{1}{2} \\ -\frac{1}{2} \\ 1 \end{bmatrix}, \quad (17)$$

with $M^{(\text{DC})} = M'_1 - M'_2$, and $M^{(\text{CLVD})} = -2M'_1$. The moment tensor elements are assumed to be arranged so that $|M'_1| \leq |M'_2| \leq |M'_3|$.

The quantity

$$\epsilon \stackrel{\text{def}}{=} \frac{-M'_1}{|M'_3|} \equiv \frac{1}{2} \frac{M^{(\text{CLVD})}}{|M^{(\text{DC})} + M^{(\text{CLVD})}|}, \quad (18)$$

is sometimes used as a measure of the departure of the deviatoric part of a moment tensor from a pure DC. It ranges in value from zero for a pure DC to $\pm 1/2$ for a

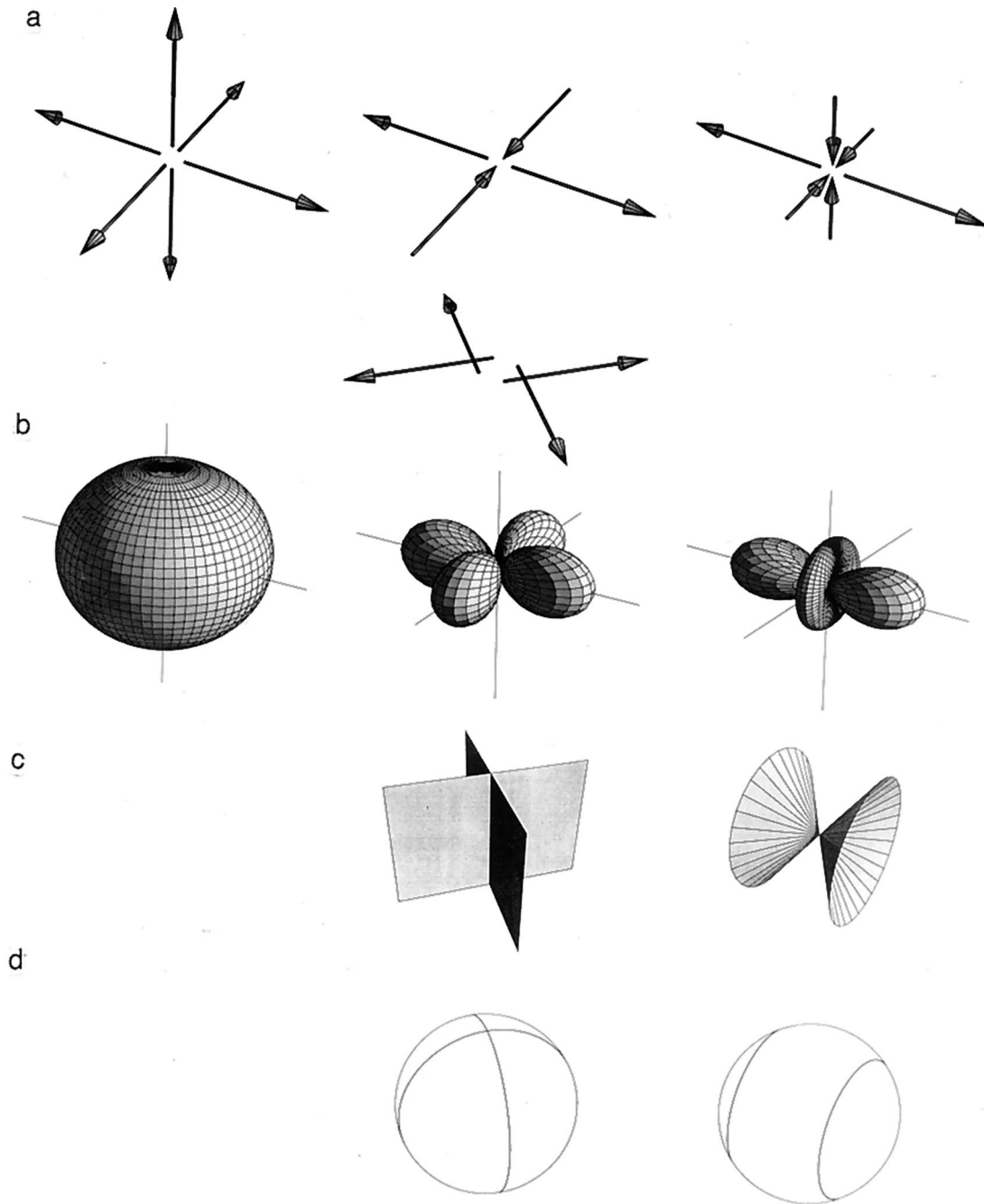


Figure 2. Three source types commonly used in decomposing moment tensors: (from left to right) isotropic, double couple (DC), and compensated linear vector dipole (CLVD). (a) Equivalent force systems, in principal axis coordinates. For the DC, the force system in a fault-oriented coordinate system is shown underneath. (b) Compressional wave radiation patterns. (c) Compressional wave nodal surfaces. (d) Curves of intersection of nodal surfaces with the focal sphere.

pure CLVD. Positive ϵ corresponds to extensional polarity for the major dipole of the CLVD component.

2.7. Displaying Focal Mechanisms

2.7.1. Focal sphere polarity maps. In Figure 3 we display focal mechanisms by showing compressional wave polarity fields on maps of the focal sphere. This representation is familiar, being widely used for DCs,

and is useful for more general (symmetric moment tensor) mechanisms as long as the principal moments are not all of the same sign (in which case one polarity field covers the entire focal sphere). *Riedesel and Jordan [1989]* proposed a way of plotting moment tensors that does not have this limitation, but it is not yet widely used.

2.7.2. Source-type plots. Both focal sphere polarity plots like those in Figure 3 and the source mechanism plots of *Riedesel and Jordan [1989]* display information

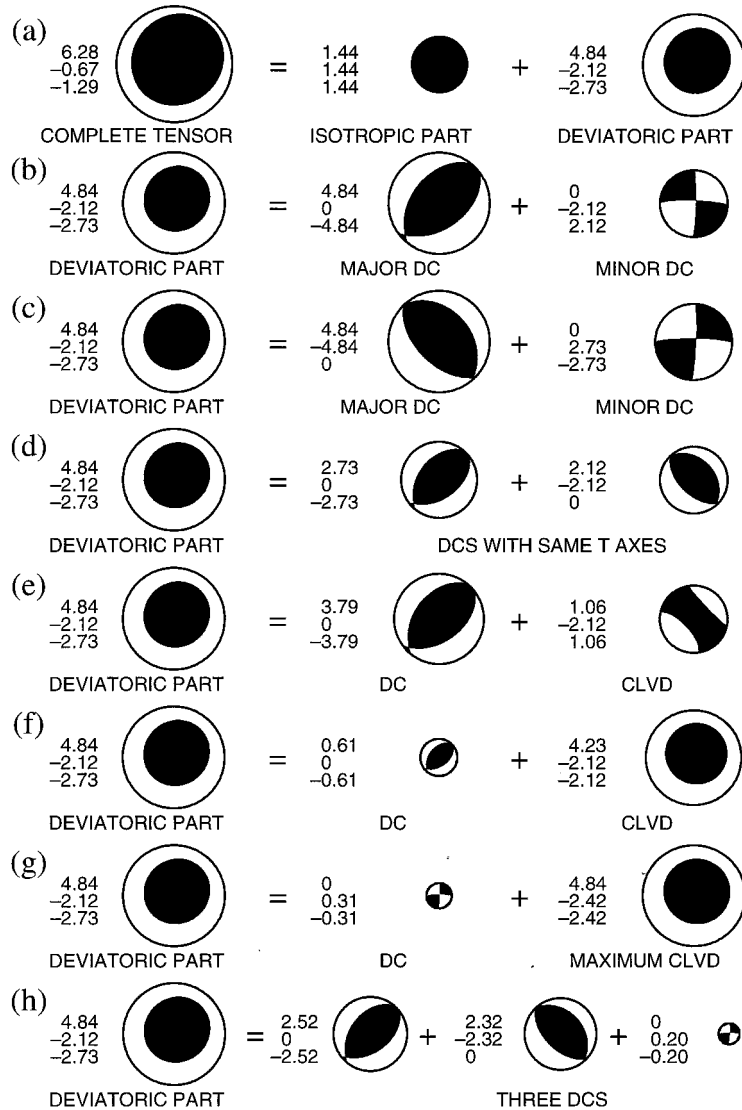


Figure 3. Some proposed methods for decomposing a general moment tensor into isotropic, DC, and CLVD parts, illustrated using the mechanism given by *Kanamori et al.* [1993, Table 1] for the Tori Shima earthquake of June 13, 1984. The area of each plot is proportional to the largest principal moment. Lower focal hemispheres are shown in equal area projection, with compressional fields shaded (compare with Figure 2d). Numbers to the left give the principal moments for each mechanism, in units of 10^{17} N m. The trends and plunges of the principal axes are $(33.7^\circ, 80.7^\circ)$, $(226.7^\circ, 9.1^\circ)$, and $(136.4^\circ, 2.1^\circ)$. (a) Decomposition into isotropic and deviatoric parts, and decompositions of the deviatoric part: (b) *Wallace* [1985, p. 11,172], (c) alternative decomposition to Figure 3b, (d) *Wallace* [1985, p. 11,172], (e) the method used in the Harvard CMT and other routine catalogs, which gives the largest possible DC that has a CLVD remainder [*Dziewonski et al.*, 1987, p. 5], (f) DC and CLVD with same T and P axes [*Knopoff and Randall*, 1970, p. 4961], (g) *Wallace* [1985, p. 11,173], and (h) *Jost and Hermann* [1989, p. 42].

about source orientation as well as “source type” (the relative values of the principal moments). In fact, conventional DC polarity plots contain information about only source orientation. When considering non-DC mechanisms, however, it is useful to display the source type without regard to orientation. The normalized principal moments contain two independent degrees of freedom, and there are many possible ways to display such information in two dimensions. Figure 4 shows the “source type plot” of *Hudson et al.* [1989], which gives -2ϵ (equation (18)) versus

$$k \stackrel{\text{def}}{=} \frac{M^{(V)}}{|M^{(V)}| + |M_3'|}, \quad (19)$$

a measure of the volume change. The projection is designed to make areas proportional to probabilities, under the a priori assumption that the principal moments M_1 and M_2 are equally likely to take any value between $-|M_3|$ and $+|M_3|$, where M_3 is the absolutely largest principal moment.

3. DETERMINING EARTHQUAKE MECHANISMS FROM OBSERVATIONS

3.1. Introduction

Many types of seismic and geodetic observations can be used to determine earthquake focal mechanisms. These range from simple determinations of the polarities (signs) of observable quantities, through measurements of their amplitudes, to complete time histories of their evolution. In this summary we concentrate on data types and analysis methods that are most useful for resolving non-DC components.

3.2. Wave Polarities

3.2.1. Classical first-motion methods. The polarity of a seismic wave contains the least information of any kind of observation (1 bit). Nevertheless, P wave polarities are the most commonly used observations in focal mechanism studies because they can be deter-

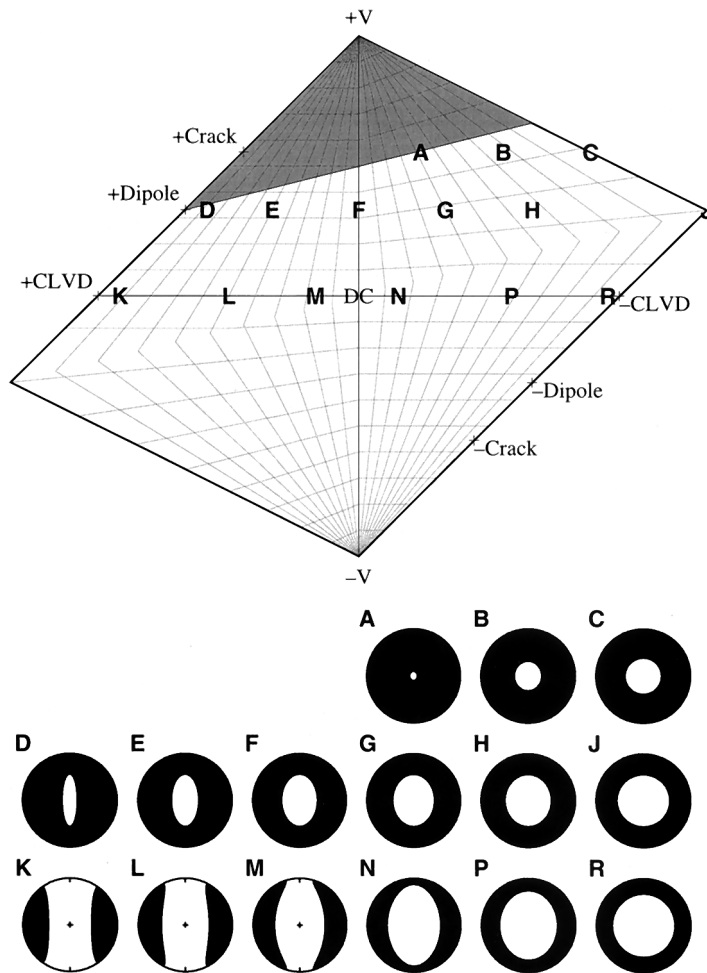


Figure 4. (top) “Source type plot” of Hudson et al. [1989], which displays earthquake mechanisms (symmetric moment tensors) without regard to their orientations. The quantity k (equation (19)), which measures volume change, ranges from -1 at the bottom of the plot to $+1$ at the top and is constant along the subhorizontal grid lines. The quantity -2ϵ (equation (18)), which describes the deviatoric part of the moment tensor, ranges from -1 on the left-hand side of the plot to $+1$ on the right-hand side and is constant along the grid lines that run from top to bottom. Notation is as follows: DC, double-couple mechanisms; +Crack, opening tensile faults; +Dipole, force dipoles with forces directed outward; +CLVD, “compensated linear-vector dipoles,” with dominant dipoles directed outward. -Crack, -Dipole, and -CLVD denote the same mechanisms with opposite polarities. The shaded area is the region in which all compressional waves have outward polarities; A similar region of inward polarities occurs at the bottom of the plot. Bold letters A–R indicate some representative mechanisms. (bottom) Conventional equal area hemisphere plots of compressional wave polarities for the 15 representative mechanisms shown on the source type plot.

mined easily, even using recordings of low dynamic range and accuracy from single-component seismometers. Such polarities alone are of very limited use, however, for studying (or even for identifying) non-DC earthquakes. Even with observations well distributed on the focal sphere, it usually is difficult to rule out DC mechanisms in practice (Figure 5). This difficulty is especially severe if the earthquake lacks a large isotropic component.

In analyzing P wave polarities, seismologists usually constrain earthquake mechanism to be DCs. Finding a DC mechanism amounts to finding two orthogonal nodal planes (great circles on the focal sphere) that separate the compressional and dilatational polarities into four equal quadrants. Three independent quantities (fault plane strike and dip angles and the rake angle of the slip vector, say) are needed to specify the orientations of the nodal planes. Nodal planes are usually sought manually, by plotting data on maps of the focal sphere and using graphical methods to find suitable nodal planes. Because humans tend to overlook alternatives once a solution has been found, computerized methods for fitting fault-plane solutions to P wave polarity distributions are now commonly used. Most of these systematically search through the space of solu-

tions [e.g., Reasenber and Oppenheimer, 1985]. (An algorithm of G. Backus (W. H. K. Lee, personal communication, 1969) for fitting fault plane solutions to P wave polarities is perhaps the earliest use of the moment tensor representation. The algorithm assigns artificial positive or negative amplitudes to the polarity observations and fits a moment tensor to these amplitudes by standard least squares methods. The DC component of the moment tensor is then taken as the fault plane solution.) All of these methods, being based on the assumption that the mechanism is a DC, are of interest primarily because their failure may indicate a non-DC earthquake.

3.2.2. Moment tensor methods. When the DC constraint is relaxed and general moment tensor mechanisms are allowed, hand fitting mechanisms to observed polarities becomes impractical. The number of unknown parameters increases from three to five (the six moment tensor components, normalized in some arbitrary way), and furthermore, theoretical nodal surfaces are no longer obtainable graphically from standard projections of the focal sphere. Searching methods still work, of course, but the addition of two more unknown parameters makes them costly in terms of computer time. The searching algorithm of Pearce and Rogers [1989] is one of

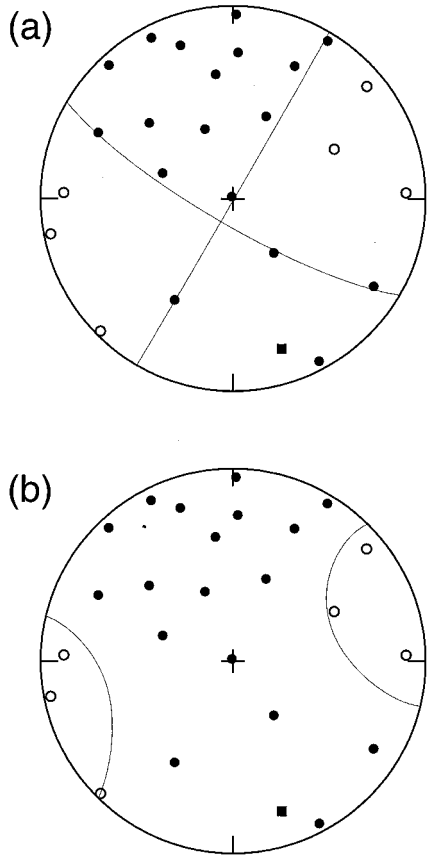


Figure 5. Illustration of the wide range of source mechanisms that typically is compatible with even a high-quality set of compressional wave polarity observations. Lower focal hemispheres are shown in equal area projection. The P -wave polarity data shown are for earthquake of 07:41 UTC, September 15, 1991 at the Hengill geothermal area, Iceland, as recorded on a network of portable digital seismometers [Julian and Foulger, 1996]. Open and solid circles indicate inward and outward motions, respectively. (a) A DC mechanism that fits all the data acceptably, considering the reliability of their focal sphere positions. (b) A more accurate mechanism, with a large isotropic component, derived by inverting body-wave polarities and amplitude ratios simultaneously (Figure 6).

the few that allow general moment tensor sources. It has been used primarily for inverting amplitude ratios (section 3.4, below) rather than polarities. Linear programming, an analytical method that treats linear inequalities, is well suited to determining moment tensors from observed wave polarities [Julian, 1986]. It is efficient and can delimit the set of solutions consistent with a data set by finding mechanisms that are extreme with respect to specified physical criteria. This method is discussed in sections 3.3 and 3.4, below.

3.2.3. Near-field polarities. When near-field observations (ones made within a few wavelengths of the source) are available, they can provide a simple and elegant method of detecting an isotropic source component using a single radial-component seismogram [McGarr, 1992; Urhammer, 1992]. The method uses the

relative polarities of different seismic phases and thus is immune to errors that reverse the polarity of the seismogram. Although the method is not guaranteed to detect isotropic components whenever they exist, it requires few assumptions, so that detected isotropic components are comparatively reliable. To illustrate the method, assume that all the moment tensor components are proportional to the unit step function $U(t)$ (any monotonic function of time will work.) Place the origin of the coordinate system at the source, with the x_1 axis directed toward the observer. (The value of the moment tensor component M_{11} appearing below thus depends on the direction to the observer.) Then from Aki and Richards [1980, equation 4.29], in an infinite medium the radial displacement (the x_1 component observed on the x_1 axis) is

$$\begin{aligned}
 u_1(t) = & \frac{3}{4\pi\rho r^4} (3M_{11} - \text{Tr}\mathbf{M})w(t) \\
 & + \frac{1}{4\pi\rho V_p^2 r^2} (4M_{11} - \text{Tr}\mathbf{M})U(t - r/V_p) \\
 & - \frac{1}{4\pi\rho V_s^2 r^2} (3M_{11} - \text{Tr}\mathbf{M})U(t - r/V_s) \\
 & + \frac{1}{4\pi\rho V_p^3 r} M_{11}\delta(t - r/V_p), \quad (20)
 \end{aligned}$$

where

$$w(t) \stackrel{\text{def}}{=} \int_{r/V_p}^{r/V_s} \tau U(t - \tau) d\tau \quad (21)$$

is a function that vanishes for $t \leq r/V_p$, increases monotonically for $r/V_p \leq t \leq r/V_s$ and is constant for $r/V_s \leq t$. Here $r \equiv x_1$ is the source-observer distance and V_p and V_s are the compressional and shear wave speeds. The near-field term (the first term on the right-hand side of (20)) therefore produces a monotonic trend on the seismogram between the compressional and shear waves. For a purely deviatoric source ($\text{Tr}\mathbf{M} = 0$), the polarity of this near-field term must be the same as that of the compressional wave (second and fourth terms). Opposite polarities on any radial seismogram imply that the source mechanism has an isotropic component. Similarly, the near-field shear wave (third term) must have the opposite polarity to the compressional wave, and any observations to the contrary indicate an isotropic source component.

3.2.4. Polarities of other seismic waves. Occasionally, the polarities of waves other than P have proven useful in source mechanism studies. For example, Toksöz and Kehler [1972] observed that the polarities of Rayleigh surface waves from underground nuclear explosions at the Nevada Test Site are sometimes reversed, and they explained this phenomenon in terms of the release of tectonic shear strain in the failure zone

around the explosion (thus turning the tables and detecting DC components in expectedly non-DC events).

3.3. Wave Amplitudes

The amplitude of a radiated seismic wave contains far more information about the earthquake mechanism than does its polarity alone, so amplitude data can be valuable in studies of non-DC earthquakes. Moreover, because seismic wave amplitudes are linear functions of the moment tensor components, determining moment tensors from observed amplitudes is a linear inverse problem that can be solved by standard methods such as least squares. Conventional least squares methods, however, cannot invert polarity observations such as first motions, which typically are the most abundant data available. Linear programming methods, which can treat linear inequalities, are well suited to inverting observations that include both amplitudes and polarities [Julian, 1978, 1986; Fitch *et al.*, 1980]. In this approach, bounds are placed on observed amplitudes, so that they can be expressed as linear inequality constraints. Polarities are already in the form of linear inequality constraints if the moment tensor representation is used.

Linear programming methods seek solutions by attempting to minimize the L1 norm (the sum of the absolute values) of the residuals between the constraints and the theoretical predictions. If all the constraints can be satisfied, a second stage of the method can be used to find those mechanisms that are extreme in terms of physically motivated linear functions of the moment tensor components such as volume change. The linear programming method is computationally efficient, typically requiring less than 1 s on a workstation to find 16 extreme mechanisms consistent with a set of a few dozen observations.

Little use has been made of seismic wave amplitudes in moment tensor studies of earthquake mechanisms. This is probably because seismologists had already shifted their attention to inverting complete waveforms before the moment tensor formalism came into widespread use [e.g., Langston and Helmberger, 1975].

3.4. Amplitude Ratios

Seismic wave amplitudes are subject to distortion during propagation, particularly because of focusing and defocusing by structural heterogeneities. A simple way to reduce the effect of this distortion when deriving earthquake mechanisms is to use as data the ratios of amplitudes of waves that have followed similar paths, such as $P:SV$, $P:SH$, or $SH:SV$. If the ratio of the wave speeds is constant in the Earth, then the amplitudes of the waves are affected similarly and the ratio is relatively unaffected.

Figure 6 shows observed $P:SH$ amplitude ratios for the same earthquake and focal mechanisms illustrated in Figure 5 [Julian and Foulger, 1996]. The use of amplitude ratios makes it clear that this earthquake is not a DC and has a large isotropic component.

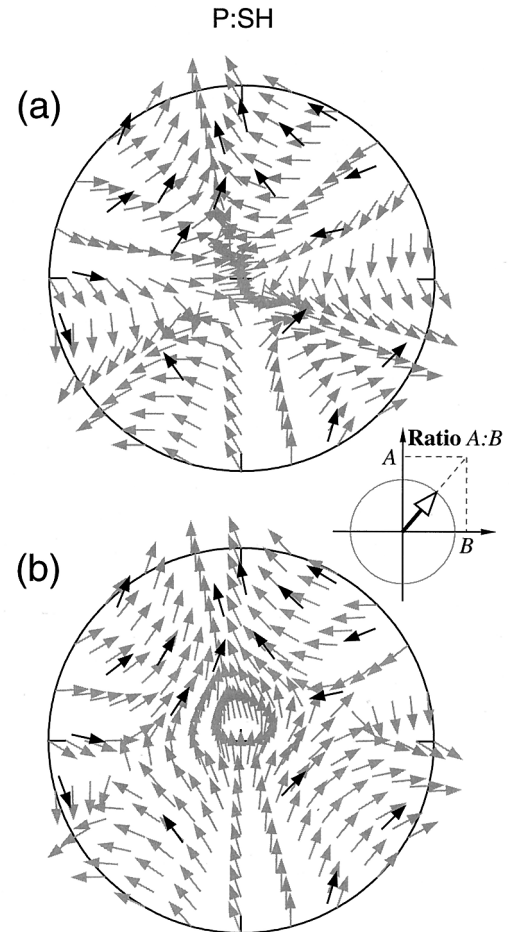


Figure 6. Use of amplitude ratios to determine focal mechanisms. Comparison of observed $P:SH$ amplitude ratios (black arrows) with theoretical ratios (gray arrows) for the (a) DC and (b) non-DC mechanisms from Figure 5. The amplitude ratios rule out a DC mechanism for this earthquake. Each ratio is represented by the orientation of an arrow (see inset). After Julian and Foulger [1996].

Using amplitude ratios makes inverting for source mechanisms more difficult, however, because a ratio is a nonlinear function of the moment tensor components. Systematic searching methods still work [Pearce and Rogers, 1989], but because the dimensionality of the model space is increased by two over that for a DC mechanism, the computational labor is greatly increased (typically by a factor of >100).

The efficient linear programming method described above is easily extended to treat amplitude ratio data in addition to polarities and amplitudes [Julian and Foulger, 1996]. (The name “linear programming” is a misnomer. The method actually deals with a class of nonlinear problems involving variables constrained to be nonnegative.) An observed ratio is expressed as a pair of bounding values, each of which gives a linear inequality that is mathematically equivalent to a polarity observation with a suitably modified Green’s function. The non-DC mechanism shown in Figure 6 was derived using this method.

3.5. Waveforms

3.5.1. Strengths and limitations. A digitized waveform is just a series of amplitude measurements, so waveform inversion may be regarded as an extension of amplitude inversion. This extension offers a great potential increase in power, however, because it can determine source time functions, which reveal the durations of earthquakes and can detect changes in mechanisms that may occur during earthquakes [Stump and Johnson, 1977]. Many algorithms in common use, however, impose constraints that preclude determining source time histories. All components of the moment tensor may be constrained to have the same time function and to differ only by constant factors, and sometimes the source time function is furthermore specified a priori, for example as a step function (so the far-field waves are impulses). Such methods are essentially equivalent to amplitude inversion, with whole waveforms being used to make more accurate measurements of amplitudes than those provided by peak values. The most severe limitation on waveform inversion methods is the need for accurate Green's functions (theoretical waveforms). It is not yet practical to compute such waveforms for realistic three-dimensional Earth models, and detailed three-dimensional models are in any case seldom available. These problems become more severe at high frequencies, so most waveform inversion studies have so far used long-period seismic waves (frequencies below ~ 0.1 Hz). It is likely that limitations imposed by Green's functions will be largely overcome in the near future by advances in methods of solving wave propagation problems in three-dimensional media.

3.5.2. Mathematical formulation. A theoretical seismogram can be written as a sum of terms, each of which is the temporal convolution of a Green's function and the time function of one source component (equation (6)). The source components can include components of the equivalent force and moment tensor components of any order. If there are n such source components (six, in the usual case of a symmetric second-rank moment tensor), which we arrange in a column vector $\Phi(t)$, then a set of m seismograms corresponds to the system of simultaneous equations

$$\begin{bmatrix} u_1(t) \\ u_2(t) \\ \vdots \\ u_m(t) \end{bmatrix} = \begin{bmatrix} A_{11}(t) & \cdots & A_{1n}(t) \\ A_{21}(t) & \cdots & A_{2n}(t) \\ \vdots & \ddots & \vdots \\ A_{m1}(t) & \cdots & A_{mn}(t) \end{bmatrix} * \begin{bmatrix} \phi_1(t) \\ \phi_2(t) \\ \vdots \\ \phi_n(t) \end{bmatrix}, \quad (22)$$

where each matrix element A_{ij} is a Green's function giving the i th seismogram generated by a source whose j th component is the impulse $\delta(t)$, and whose other components are zero. The asterisk indicates temporal convolution. The Green's functions can be thought of as a multichannel filter that takes the n source time functions $\phi_i(t)$ as inputs and generates as output the m synthetic seismograms $u_i(t)$.

Estimating the source time functions from a set of observed seismograms and assumed Green's functions is thus a multichannel inverse filtering, or deconvolution, problem. It can be solved, for example, by transforming to the frequency domain (so that the convolutions become multiplications) and then applying standard least squares methods to solve for each spectral component. Alternatively, the output seismograms in (22) can be concatenated into a single time series, and the Green's functions in each column of the matrix A can be similarly concatenated. Then when each time series is expressed explicitly in terms of its samples, the least squares normal equations turn out to have a "block-Toeplitz" structure, so that they can be solved efficiently by Levinson recursion [Sipkin, 1982].

Usually, however, the problem is simplified by (1) assuming that all the source components have the same time functions and differ only by constant factors, and perhaps by (2) assuming a simple functional form for the source time function and solving for a small number of parameters (e.g., rise time, duration) appearing in this functional form. Such simplifying assumptions, though greatly reducing computational labor, are poorly suited to investigating unknown source processes such as those on non-DC earthquakes, for which they may not hold.

3.5.3. Routine analyses. Harvard University, the U.S. Geological Survey (USGS), and the Earthquake Research Institute of Tokyo University all routinely determine moment tensors for large earthquakes throughout the world in near-real time and distribute the results via global computer networks within a few hours of the occurrence of an earthquake. Harvard and the USGS later analyze more complete data sets and publish the results in the *Bulletin of the International Seismological Centre* and in the USGS *Preliminary Determination of Epicenters (PDE)* bulletin. Harvard and the USGS also publish their final solutions regularly in the journal *Physics of the Earth and Planetary Interiors*. All of these groups, unfortunately, constrain mechanisms to be purely deviatoric. All of them also decompose moment tensors in a manner that is ill suited to the study of non-DC processes [Dziewonski et al., 1987, page 5] (section 2.6).

Harvard University began regular computation of centroid moment tensor (CMT) solutions with earthquakes of 1982. Solutions for 401 earlier earthquakes, going back to 1977, are given by Dziewonski and Woodhouse [1983] and Giardini [1984]. By now, more than 10,000 solutions have been published. Solutions are derived from body wave portions of seismograms and, except for the smallest events, also from mantle waves, using methods described by Dziewonski et al. [1981] and Dziewonski and Woodhouse [1983]. Harvard is the only one of the three institutions that publishes earthquake source durations, but these are values determined from seismic moments using an empirical formula and are not measured values. Error bounds, but not complete covariance information, are given for the moment tensor

elements. No information is given about the quality of fit to the data that was achieved. For an explanation of the published tables, see *Dziewonski et al.* [1987].

The U.S. Geological Survey also began regular determination of global moment tensor solutions in 1982, and rapid determinations began in May 1993 [*Sipkin*, 1994]. In order to obtain solutions as quickly as possible, the USGS uses only the P wave group (including the surface-reflected phases pP and sP) in its analysis. Before inversion, observed and theoretical waveforms are aligned in time, to reduce the effects of timing errors, epicentral mislocation, and three-dimensional Earth structure. Therefore the epicentral coordinates do not correspond to the moment centroid. Focal depths are determined by finding the depth that best fits the observed waveforms, and correspond closely to centroid depths. No information is given about probable uncertainties in moment tensor components. Measures of the quality of fit to the data are, however, published in the periodic summaries in *Physics of the Earth and Planetary Interiors*.

The Earthquake Research Institute of Tokyo University began computing centroid moment tensors in October 1993, using a method similar to that of Harvard [*Kawakatsu et al.*, 1994; *Kawakatsu*, 1995]. This procedure is completely automated, and its speed is limited primarily by data acquisition, although the method is still in the experimental stage. Because solutions are not reviewed by seismologists prior to distribution, they are accompanied by information about the quality of fit to the data that was achieved. Confidence intervals, but not complete covariance information, are given for the moment tensor elements.

3.6. Limitations

3.6.1. Imperfect Earth models. If the Earth model used to analyze the radiation from an earthquake differs from the true structure of the Earth, systematic errors will be introduced into the Green's functions and thus into inferred source mechanisms. Near-source anisotropy, discussed in section 4.4 below, is one cause of such errors. Some types of observations, such as those of SV waves, are particularly sensitive to Earth model errors.

The component of a shear wave polarized in the vertical plane tangential to the ray emerging at the surface (the SV wave) is subject to distorting effects that limit its usefulness. (1) Strong heterogeneity near the surface causes some of the energy of the SV wave to be converted to compressional waves. These converted waves arrive at the sensor slightly before the direct wave and tend to obscure its true arrival time, amplitude, and waveform. (2) When the SV wave is incident beyond the critical angle (so that the reflected compressional wave is evanescent), the waveform becomes complicated and nearly useless for source mechanism investigation. This effect limits the usefulness of SV waves to epicentral distances that are either less than about the focal depth

(within the “shear wave window”) or beyond about 44° . Shear waves polarized horizontally (SH waves) do not suffer from either of these problems.

3.6.2. Deficient combinations of modes. Even if the Green's functions are correct, it may be impossible to determine the source mechanism completely in some circumstances. For particular types of seismic waves, there may be certain source characteristics that cannot be determined. For example, shear waves alone cannot detect isotropic source components because purely isotropic sources do not excite shear waves. Similarly, sources with vertical symmetry axes (those whose only nonzero components are $M_{11} = M_{22}$ and M_{33} , with the x_3 axis vertical) excite no horizontally polarized shear (SH) or Love waves and cannot be detected using such waves alone. For any Rayleigh mode the component M_{33} occurs only in the combination $M_{11} + M_{22} + f(\omega)M_{33}$, where the frequency function $f(\omega)$ depends on the mode and the Earth model. The M_{33} component can be traded off against $M_{11} + M_{22}$ without changing this combination, so isotropic sources are unresolvable by Rayleigh waves of a single frequency and mode [*Mendiguren*, 1977], and even with multimode observations, determining M_{33} requires a priori assumptions about its spectrum. In most studies, enough different modes and/or frequencies are used so that none of these degenerate situations arises. Furthermore, all general inversion methods in widespread use provide objective information about uncertainty and nonuniqueness in derived values, so degeneracies can be detected if they happen to occur.

3.6.3. Shallow earthquakes. If an earthquake is effectively at the free surface (shallow compared to the seismic wavelengths used), then it becomes impossible to determine its full moment tensor. Only three moment tensor components can be determined, and these are not enough even under the a priori assumption of a DC mechanism (which requires four parameters). This degeneracy follows from the proportionality between the coefficient C_{ij} giving the amplitude of a seismic mode excited by the moment tensor component M_{ij} and the displacement derivative $u_{i,j}$ for the mode. (This proportionality follows from the principle of reciprocity.) The vanishing of the traction on the free surface,

$$\begin{aligned}\sigma_{13} &= \mu(u_{1,3} + u_{3,1}) = 0, \\ \sigma_{23} &= \mu(u_{2,3} + u_{3,2}) = 0,\end{aligned}\quad (23)$$

$$\sigma_{33} = \lambda(u_{1,1} + u_{3,3}) + (\lambda + 2\mu)u_{3,3} = 0,$$

therefore implies that three linear combinations of the excitation coefficients must vanish:

$$\begin{aligned}C_{13} &= 0, \\ C_{23} &= 0,\end{aligned}\quad (24)$$

$$\lambda C_{11} + \lambda C_{22} + (\lambda + 2\mu)C_{33} = 0.$$

(Here we restrict ourselves to symmetric moment tensors.) It follows that a moment tensor whose only non-zero components are M_{13} and M_{23} radiates no seismic waves (to this order of approximation) and, moreover, that a diagonal moment tensor with elements in the ratio $\lambda:\lambda:(\lambda + 2\mu)$ likewise radiates no seismic waves. The first case corresponds to a vertical dip-slip shear fault or a horizontal shear fault, and the second corresponds to a horizontal tensile fault. This second undeterminable source type has an isotropic component, so isotropic components cannot be determined for shallow sources. It is common practice to choose the undetermined moment tensor components so as to make the source a DC, at the same time minimizing the magnitudes of the introduced components.

This degeneracy is most often important in studies using surface waves or normal modes, because these are usually observed at frequencies below 0.05 Hz, for which the wavelengths are greater than the focal depths of many earthquakes. Observations of this sort are sometimes used in studies of regional tectonics, but such use requires assumptions that are incompatible with investigating non-DC mechanisms.

For very shallow earthquakes the free surface effect can significantly distort higher-frequency waves as well. Normal-faulting earthquakes on mid-ocean ridges, for example, often yield teleseismic fault plane solutions with nonorthogonal nodal planes [Sykes, 1967, 1970], which have been misinterpreted as evidence of refraction of rays around hypothetical magma chambers beneath the ridge [Solomon and Julian, 1974]. The observations in such cases are explained adequately in terms of interference between direct P waves and the surface-reflected phases pP and sP , which arrive at nearly the same time and cause first motions to be determined incorrectly [Hart, 1978].

4. POSSIBLE NON-DC EARTHQUAKE PROCESSES

4.1. Processes Involving Net Forces

4.1.1. Physical principles. Most experimental investigations of earthquake source mechanisms have excluded net forces and torques from consideration a priori. As was discussed in section 2.2.2, the laws of physics do not require such restrictions. Net forces are possible for an internal source because momentum can be transferred between the source region and the rest of the Earth. Momentum conservation does, however, require that the impulse (time integral) of the net force component must vanish if the source is at rest before and after the event.

4.1.2. Landslides. Among sources that involve net forces, landslides have received the most attention. Modeling a landslide as a block of mass M sliding down a ramp of uniform slope gives an equivalent force of $-Ma$, where \mathbf{a} is the acceleration of the block [Hasegawa

and Kanamori, 1987; Kawakatsu, 1989; Dahlen, 1993]. The force is thus parallel to the slope, in the direction opposite to the motion while the slide is accelerating and in the same direction while the slide is decelerating.

The gravitational forces on a landslide also produce a torque of magnitude $mg\Delta x$, where g is the acceleration of gravity and Δx is the horizontal distance the slide travels. This torque can be substantial. The May 18, 1980, eruption of Mount St. Helens, for example, was accompanied by a landslide with a mass of about 5×10^{13} kg that traveled a horizontal distance of about 10 km [Voight et al., 1981]. These values correspond to a net torque of about 5×10^{18} N m. By comparison, the two largest earthquakes accompanying the eruption had surface wave magnitudes of about 5.3 [Kanamori and Given, 1982], which correspond to seismic moments of about 2.6×10^{17} N m [Miller et al., this issue]. Apparently, no seismological analyses of landslides to date have included such torques in the source mechanism.

4.1.3. Volcanic eruptions. The eruption of material by a volcano applies a net force to the Earth, much as an upward directed rocket exhaust would. Of course, the total impulse imparted to the Earth-atmosphere system is zero, as with any internal source, but the spatially and temporally concentrated force at the volcanic vent can generate observable seismic waves, whereas the balancing forces transmitted from the ejected material through the atmosphere back to the Earth's surface excite waves that are probably unobservable in practice. Therefore a volcanic eruption may be modeled as a point force $S\Delta P$, where S is the area of the vent and ΔP is the pressure difference between the source reservoir within the volcano and the atmosphere [Kanamori et al., 1984].

Other processes accompanying volcanic eruptions might act as seismic wave sources. A change in pressure in a spherically symmetric reservoir acts as an isotropic source with a moment tensor given by equation (15) (section 2.5). For a tabular or crack-shaped reservoir, the force system is the same as that for a tensile fault, discussed in sections 2.4.3 and 4.3.

4.1.4. Unsteady fluid flow. Other possible volcanic source processes include unsteady fluid flow in volcanic channels. If the speed, and thus the momentum, of magmatic fluid flowing in a volcanic conduit varies with time, a time-varying net force,

$$\mathbf{F} = - \iiint_V \rho \mathbf{a} dV, \quad (25)$$

is exerted on the surrounding rocks, where ρ is the density of the fluid and \mathbf{a} is its acceleration (Figure 7). This process may cause "long-period" volcanic earthquakes [Ukawa and Ohtake, 1987] and the closely related phenomenon of volcanic tremor [Julian, 1994]. Time variations in the flow speed might be caused by the breaking of barriers to flow, or be self-excited by non-

linear interaction between the flowing fluid and the deformable channel walls [Julian, 1994].

4.2. Complex Shear Faulting

4.2.1. Multiple shear events. If earthquakes occur close together in space and time, observed seismic waves may not be able to resolve them, and they may be misinterpreted as a single event. The apparent moment tensor of the composite event is then the sum of the true moment tensors of the earthquakes, and because the sum of two DCs is not, in general, a DC, shear faulting can produce non-DC mechanisms in this way. Not all combinations of earthquake mechanisms give non-DC resultants, however, and in fact many of the most likely combinations have composite mechanisms that are DCs, including earthquakes with (1) parallel fault planes, (2) parallel slip directions, or (3) parallel intermediate principal axes (null axes). Important special cases that sum to produce DCs include cylindrical faults with slip parallel to the axis (case 2) or perpendicular to the axis (case 3) [Frohlich *et al.*, 1989; Frohlich, 1990], listric, or “sled runner” faults (case 3), and conjugate faults (case 3). Of course, combining DCs cannot ever produce mechanisms with isotropic (volume change) components, because the trace of the moment tensor is a linear function of its components. Multiple shear-faulting mechanisms therefore lie on the horizontal ($k = 0$) axis of source-type plots.

Some particular geological environments may favor fault geometries that give non-DC composite mechanisms. For example, most earthquakes in subducted lithospheric slabs have mechanisms with the P or T axis in the downdip direction. A combination of such an earthquake and an earthquake caused by bending stresses near the slab surfaces can have a non-DC composite mechanism [Frohlich *et al.*, 1989]. Similarly, a combination of a normal-faulting earthquake on a mid-ocean ridge and a strike-slip earthquake on a transform

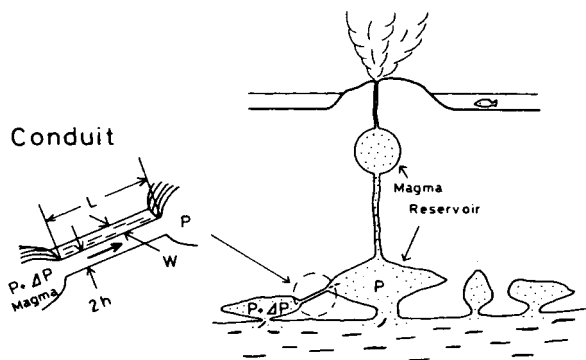


Figure 7. Schematic view of magma-transporting channels within a volcano [from Ukawa and Ohtake, 1987]. Time-varying fluid advection, whose source mechanism includes net forces, may cause “long-period” volcanic earthquakes and volcanic tremor.

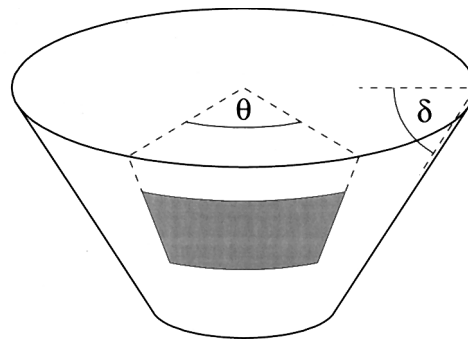


Figure 8. Geometry of volcanic ring faulting used in computing mechanisms shown in Figure 9. Dip-slip motion on fault of dip δ is uniformly distributed over azimuth range θ .

fault gives a non-DC composite mechanism [Kawakatsu, 1991].

By analyzing complete seismic waveforms, rather than just polarities or amplitudes, it is often possible to identify cases of complex shear faulting by resolving a multiple event into subevents with different mechanisms. This requires use of algorithms that allow the moment tensor to vary with time in a general way [Sipkin, 1986]. Many algorithms for inverting waveforms, however, assume that all the moment tensor components have identical time functions and may even make a priori assumptions about what this function is. In such cases, even if the subevents have identical DC mechanisms, the apparent mechanism can have a spurious non-DC component [Sipkin, 1986].

4.2.2. Volcanic ring faults. Dikes intruded along conical surfaces with both outward and inward dips are often found in exhumed extinct volcanoes and are expected consequences of the stresses caused by inflation and deflation of magma chambers [Anderson, 1936]. These dikes are of two types: “cone sheets,” which dip inward at $\sim 30^\circ$ – 70° , and are thought to form as tensile faults during inflation, and nearly vertical or steeply outward dipping “ring dikes,” which form through shear failure accommodating subsidence following deflation or eruption of magma. For both types the axes of the cones are approximately vertical. In a few cases, microearthquake locations at active volcanoes show evidence of current activity on such structures, for example on near-vertical faults at Rabaul caldera on New Britain [Mori and McKee, 1987]. If dip-slip shear faulting occurs on a conical fault, and the rupture in an earthquake spans a significant azimuth range (Figure 8), the resulting mechanism, considered as a point source, can have a non-DC component [Ekström, 1994]. (Strike-slip motion on such a surface always gives pure DC mechanisms.) Figure 9 shows a suite of theoretical source mechanisms corresponding to dip-slip ruptures spanning various azimuth ranges on conical faults of different dips. For steeply dipping faults the non-DC components are small (for vertical faults they vanish), so cone sheets are more efficient than ring dikes as sites for this non-DC process.

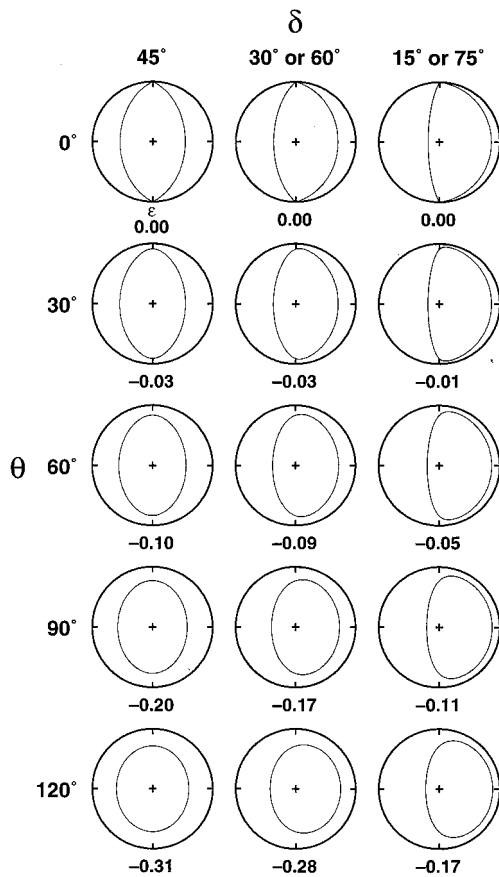


Figure 9. Non-DC mechanisms for volcanic ring faulting (Figure 8). Theoretical compressional wave nodal surfaces for an arcuate dip-slip fault whose strike spans a range θ and averages north-south. Each focal sphere corresponds to two situations: a fault dipping to the west by the smaller angle δ given or to the east by the larger angle. All mechanisms are purely deviatoric. Numbers below each mechanism give values of ϵ (equation (18)), which describe the deviatoric parts of the moment tensors. Upper focal hemispheres are shown in equal area projection. Lower hemisphere plots are left-right mirror images. For normal faulting (upper block moving down), central fields have dilatational polarity.

4.3. Tensile Faulting

4.3.1. Opening tensile faults in the Earth. An obvious candidate mechanism for geothermal and volcanic earthquakes is tensile faulting, in which the displacement discontinuity is normal, rather than parallel, to a fault surface. The equivalent force system of a tensile fault consists of three orthogonal linear dipoles with moments in the ratio $(\lambda + 2\mu) : \lambda : \lambda$. It is equivalent to an isotropic source of moment $(\lambda + 2\mu/3)A\bar{u}$ plus a CLVD of moment $(4\mu/3)A\bar{u}$ (section 2.4.3). The far-field compressional waves have all first motions outward, with amplitudes largest (by a factor of $1 + 2\mu/\lambda$) in the direction normal to the fault. Figure 4 shows the position of tensile faults on a source-type plot.

Compressive stress tends to prevent voids from forming at depth in the Earth, but high fluid pressure can

overcome this effect and allow tensile failure to occur. The situation is conveniently analyzed using Mohr's circle diagrams (Figure 10). The effect of interstitial fluid at pressure p in a polycrystalline medium such as a rock is to lower the effective principal stresses by the amount p . Thus fluid pressure, if high enough, can cancel out much of the compressive stress caused by the overburden. Fluid pressures comparable to the lithostatic load are found surprisingly often in deep boreholes.

A second prerequisite for tensile failure is that the shear stresses be small, or equivalently that the principal stresses be nearly equal. The diameter of the Mohr's circle in Figure 10 is equal to the maximum shear stress (difference between the extreme principal stresses). If this diameter is too large, the circle can touch the failure envelope only along its straight portion, which corresponds to shear failure. Only if the shear stress, and thus the diameter, is small will the circle first touch the failure envelope in the tensile field to the left of the τ axis.

4.3.2. Crack dynamics. In theory, a fluid-driven tensile fault in an infinite homogeneous medium cannot propagate faster than the fluid can flow, and therefore

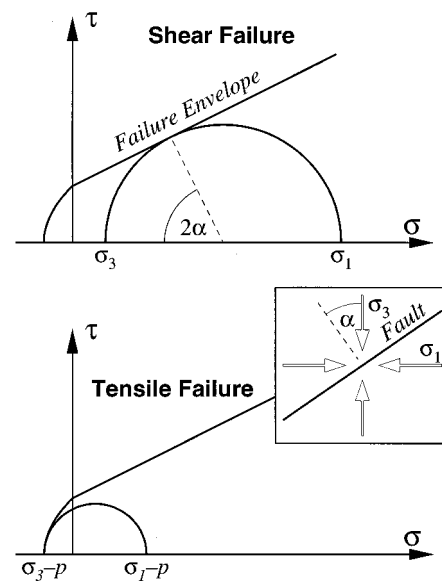


Figure 10. Conditions for shear and tensile failure (adapted from Julian and Sipkin [1985, Figure 16]). Mohr's circle diagram shows the relationship between shear traction τ and normal traction σ across a plane in a stressed medium. Locus of (σ, τ) points for different orientations of the plane is a circle of diameter $\sigma_1 - \sigma_3$, centered at $((\sigma_1 + \sigma_3)/2)$, where σ_1 and σ_3 are the extreme principal stresses. Failure occurs when circle touches the "failure envelope", and the point of tangency determines the orientation of the resulting fault (see inset). (The theoretical failure envelope shown corresponds to Griffith theory of failure, as modified by F. A. McClintock and J. B. Walsh [Price, 1966].) The straight portion of the failure envelope in the compressional field ($\sigma > 0$) represents the Navier-Coulomb criterion for shear failure. (top) At high confining stress with no fluid pressure, only shear failure occurs. (bottom) High fluid pressure lowers the effective confining stress, and tensile failure occurs for low stress differences.

cannot radiate elastic waves and cause an earthquake. This is because a fault propagates only when the stress intensity at its tip exceeds a critical value, the fracture toughness of the rock. If the fault tip propagates ahead of the driving fluid, the stress intensity decreases and propagation stops until the fluid again reaches the tip.

Departures from heterogeneity can change the situation radically, however, and make tensile faults unstable and able to propagate ahead of the driving fluid at elastic wave speeds and cause earthquakes. In particular, tensile faults propagate unstably when they (1) approach a free surface (and probably also regions of low elastic modulus), (2) approach other tensile faults, and (3) initially propagate outward from magma chambers [Sammis and Julian, 1987].

4.3.3. Effects of fluids. As discussed above, the compressional waves radiated by an opening tensile fault are expected to have compressive (outward) first motions for all observation directions. The subsequent migration of fluid into the fault, however, will superimpose a slightly delayed dilatational signal. In seismological observations with wavelengths larger than the source dimensions, these two signals will be indistinguishable, and the effect of fluid motion may be to reverse the apparent first motion polarities for observations near the plane of the fault [Foulger and Long, 1984]. In numerical models of propagating fluid-filled tensile faults, the dilatational signals are always too weak to cause such reversal, however [Chouet and Julian, 1985; Chouet, 1986].

4.3.4. Fault-opening slip pulses. In laboratory studies, shear faulting in foam rubber models often involves transient separation of the fault surfaces [Brune et al., 1993]. The mechanism by which this occurs is poorly understood, but the opening facilitates slippage and decreases the amount of heat generated [Anooshehpour and Brune, 1992, 1994]. If a similar mechanism occurs in nature, it might resolve some current paradoxes about faulting, such as how faults can slip under extremely low driving shear stresses [Zoback et al., 1987] and why friction does not produce large heat flow anomalies near major faults [Lachenbruch and Sass, 1980]. Because the opening is transient, with the fault surfaces closed both before and after an earthquake, this phenomenon will not contribute to moment tensors of temporal order zero. Only explicitly time-dependent or higher-order temporal moments can represent transient opening. As studies using such source descriptions become more common, they may provide evidence about whether slip on natural faults is facilitated by this mechanism.

4.3.5. Combined tensile and shear faulting. Although tensile faults could cause earthquakes that involve volume increases, they cannot explain non-DC earthquakes whose isotropic components indicate volume decreases. Tensile faults can open suddenly for a variety of reasons (section 4.3.2), but they would be expected to close gradually and not to radiate elastic

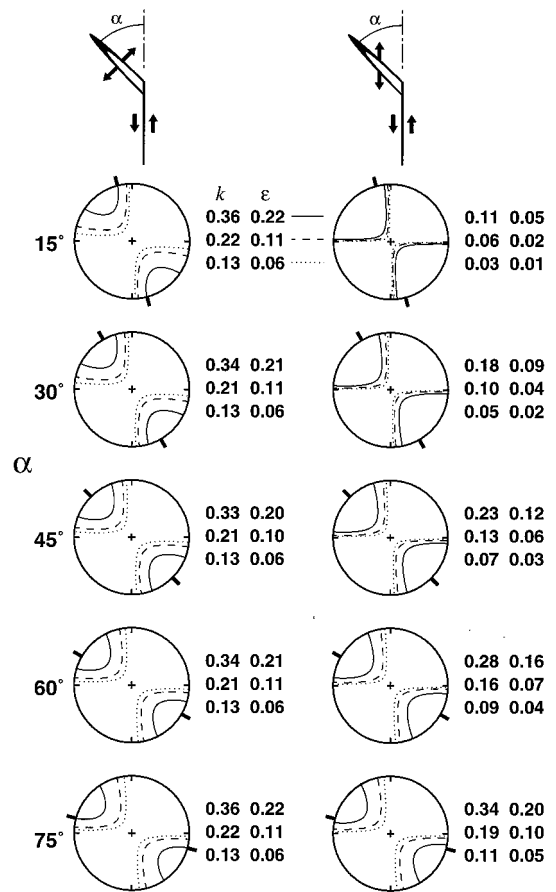


Figure 11. Non-DC mechanisms for combined tensile and shear faulting with different geometries. Both faults are vertical, with the shear fault striking north-south and the tensile fault striking west of north at the angle α , indicated by bold ticks. (left) Tensile fault opening normal to its face. (right) Tensile fault opening obliquely, parallel to the shear fault. Compressional wave nodal surfaces are shown for different relative moments of the tensile (M^T) and shear (M^S) components. Solid curves are for $M^T = 0.5M^S$, dashed curves are for $M^T = 0.2M^S$, and dotted curves are for $M^T = 0.1M^S$. Numbers to the right of each plot give values of k and ϵ (equations (19) and (18)) for each mechanism. Focal hemispheres (either upper or lower, because of symmetry) are shown in equal area projection.

waves. If a tensile fault and a shear fault intersect, however [Shimizu et al., 1987], then stick-slip instability could cause sudden episodes of either opening or closing, with volume increases or decreases. The stresses around the tips of both shear and tensile faults favor this type of fault pairing. A similar type of mixed faulting occurs in rocks subjected to strain in the laboratory [Brace et al., 1966; Scholz, 1990, section 1.2.3.]. A similar situation can occur in the case of shear faulting near mines, with the tunnel playing the role of the tensile fault.

Figure 11 shows the theoretical source mechanisms for combined tensile and shear faults of different geometries and relative seismic moments. When the tensile fault opens or closes in the direction normal to its face,

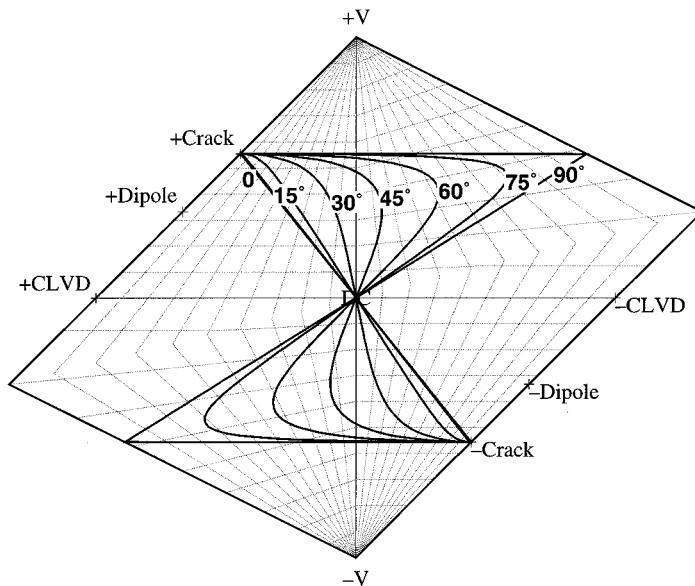


Figure 12. Source types for combined tensile and shear faulting. Numbers give angles between the tensile fault planes and the intermediate principal (null) axes of the shear faults. Small angles are physically most plausible. (For the mechanisms shown in Figure 11 this angle is zero.) For all possible relative orientations and moments, the source type lies between the corresponding curve and the straight line from +Crack to -Crack. The upper half of the plot corresponds to opening faults, and the lower half corresponds to closing faults. For an explanation of the plotting method, see Figure 4.

the mechanisms have large isotropic components, with most of the focal sphere having the same polarity as the tensile fault and two unconnected fields having the opposite polarity. The symmetry of the moment tensors makes it impossible to determine the angle between the two faults. An angle of $45^\circ - x$ is equivalent to an angle of $45^\circ + x$. When the tensile fault opens or closes obliquely, in the direction parallel to the shear fault, then the mechanisms are closer to DCs and less sensitive to the relative seismic moments.

If the dominant principal axis of the tensile fault lies in the same plane as the P and T axes of the shear fault (i.e., if the null axis of the shear fault lies in the tensile fault plane), then the composite mechanism lies on the line between the DC and Crack positions on a focal sphere plot. For more general (and less physically plausible) geometrical arrangements, the composite mechanism lies within a region consisting of two triangles (Figure 12).

4.4. Shear Faulting in an Anisotropic Medium

The equivalent force system of an earthquake depends on the constitutive law used to compute the model stress s_{ij} in equation (2). This means that a fault in an anisotropic elastic medium has a different equivalent force system than it would if the medium were isotropic and, in particular, that a shear fault in an anisotropic medium generally has a non-DC moment tensor, which can be determined, for example, from (13). Most rocks are seismically anisotropic because of such effects as layering on a scale smaller than seismic wavelengths [Backus, 1962], preferential orientation of crystals, and the presence of cracks and inclusions [Leary et al., 1990], so most earthquakes should have non-DC mechanisms because of anisotropy.

Elastic wave propagation in an anisotropic medium is more complicated in several ways than in an isotropic

medium. The particle motion in body waves is no longer either longitudinal or transverse to the direction of propagation but is generally oblique, so body wave modes are referred to as “quasi-compressional” and “quasi-shear.” The “direction of propagation,” in fact, is no longer a single direction, but rather two directions for each mode: the normal to the wavefront (the “phase velocity” direction) and the direction of energy transport (the “group velocity” direction, from the source to the observer).

Of course, Green’s functions for the anisotropic medium must be used to compute the radiated seismic waves for the force system given by equation (13) and to solve the inverse problem of determining the force system from observed seismograms. If enough information is available about source region anisotropy to determine such Green’s functions, then it will be possible to recognize when non-DC force systems are consistent with shear faulting. In practice, however, information about anisotropy in earthquake focal regions is seldom available, so Green’s functions appropriate for isotropic constitutive laws are used instead. In this case the non-DC force system of most interest is not the one given by (13), but rather the one that would be derived from seismic waves using an isotropic constitutive law when the focal region is actually anisotropic.

Figure 13 shows compressional wave nodal surfaces computed by Kawasaki and Tanimoto [1981] for a shear fault in a medium with orthorhombic anisotropy appropriate for single-crystal olivine. The anisotropy in this model is stronger than would be appropriate for mantle rocks, which are polycrystalline aggregates including pyroxenes and other minerals and having olivine crystals preferentially but not perfectly oriented. The nodal curves indicate that the effect of anisotropy is strong enough to be significant in well-constrained experiments. The figure also indicates that anisotropic Green’s functions must be used to obtain accurate nodal posi-

tions. If nodal surfaces are computed with correct (anisotropic medium) moment tensors but isotropic-medium Green's functions, they are subject to errors comparable to the non-DC effect being studied.

Nodal surfaces do not tell the whole story, however. Source region anisotropy can cause large variations in seismic wave amplitudes even when it does not affect the nodal positions. Figure 14, for example, shows the theoretical radiation patterns of quasi-compressional and quasi-shear waves for a DC force system in a medium with moduli derived from measurements on peridotites thought to be derived from the upper mantle [Gajewski, 1993]. (This DC source does not, of course, correspond to shear faulting, because the medium is anisotropic.) For observations in a plane of symmetry of the medium, the nodal locations are about the same as for isotropic media, but the quasi-SV amplitudes differ greatly from the SV amplitudes in the isotropic case. For observations outside the symmetry planes, the radiated amplitudes differ greatly from the isotropic case and the radiation pattern does not even have the same number of lobes, although some of the nodal positions remain the same. It is clear the effects of source-region anisotropy are significant and should be taken into account, especially in studies using seismic wave amplitudes.

4.5. Shear Faulting in a Heterogeneous Medium

If an earthquake occurs in a place where the elastic moduli vary spatially, its apparent mechanism will be distorted, and a DC earthquake may appear to have non-DC components. This occurs when the spatial derivatives of Green's functions (strains) appearing in the second term on the right side of the moment expansion (6) vary significantly over the source region, so that the values at $\xi = \mathbf{0}$ are inappropriate for a portion of the moment release. In effect, neglected higher moments are contaminating estimates of the lower moments.

This effect is not a consequence of using an incorrect Earth model to compute the Green's function. In this discussion we assume that the Earth model and Green's function are exact. The distortion of the focal mechanism is caused by the finiteness of the source region. Errors in the Green's function due to our incomplete knowledge of Earth structure and to the mathematical complexity of elastodynamics can of course cause severe errors in derived earthquake mechanisms, but that is not the phenomenon under discussion here.

Consider an earthquake near an interface across which the elastic moduli change discontinuously [Woodhouse, 1981], so that the truncated Taylor series (equation (5)) is a particularly poor approximation. Then the inferred mechanism of an earthquake that is assumed to occur on one side of the interface will be distorted if the earthquake actually is on the other side. If the source region includes both sides of the interface, it is unavoidable that a portion of the moment release will be distorted in this manner.

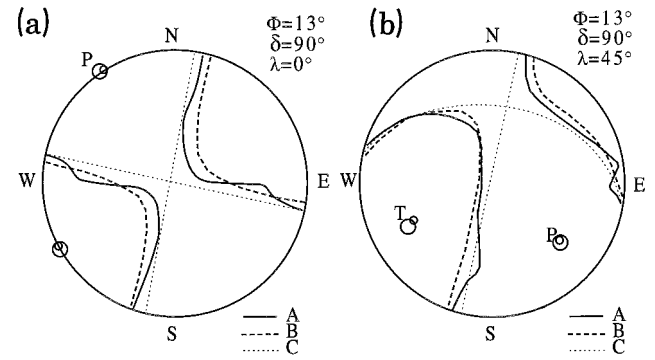


Figure 13. Quasi-compressional wave nodal surfaces for shear faults in an anisotropic medium [from *Kawasaki and Tanimoto, 1981*]. The medium has elastic moduli appropriate for single-crystal olivine (orthorhombic symmetry), with a axis vertical, b axis horizontal and trending $N103^\circ E$, and c axis horizontal and trending $N13^\circ E$. Faulting occurs on the a - c plane (strike 13° , dip 90°). (a) Strike-slip faulting (rake = 0°). (b) Oblique faulting (rake = 45°). Large circles indicate principal moment directions; Small circles indicate principal moment directions for DCs appropriate for an isotropic medium. Solid and dashed lines show the nodal surfaces computed using moment tensor and Green's function for an anisotropic medium, and an isotropic medium, respectively; dotted lines show the nodal surfaces for Green's function and DC mechanism appropriate for an isotropic medium. Lower focal hemispheres are shown in equal area projection.

If we arrange the independent components of the moment tensor in a column vector,

$$\mathbf{m} \stackrel{\text{def}}{=} [M_{11} \ M_{12} \ M_{22} \ M_{13} \ M_{23} \ M_{33}]^T, \quad (26)$$

then the seismic waves excited can be written $\mathbf{g}^T \mathbf{m}$, where \mathbf{g} is a column vector whose components are spatial derivatives of Green's functions appearing in the second term on the right side of (6). Because displacement and stress are continuous at the interface, the elements of \mathbf{g} on one side of the interface are related to those on the other side by a relation that can be written

$$\mathbf{A}^+ \mathbf{g}^+ = \mathbf{A}^- \mathbf{g}^-, \quad (27)$$

where \mathbf{A} is a matrix that depends on the orientation of the interface and the elastic moduli adjacent to it, and the plus and minus superscripts indicate values on the two sides of the interface. It follows that

$$\mathbf{g}^{+T} \mathbf{m} = \mathbf{g}^{-T} [\mathbf{A}^{+-1} \mathbf{A}^-]^T \mathbf{m}, \quad (28)$$

or in other words, that an earthquake with moment tensor \mathbf{m} occurring on the "plus" side of the interface excites the same waves as an earthquake with moment tensor $[\mathbf{A}^{+-1} \mathbf{A}^-]^T \mathbf{m}$ occurring on the opposite ("minus") side. In a coordinate system with the x_3 axis normal to the interface, the matrix connecting the true and apparent moment tensors is

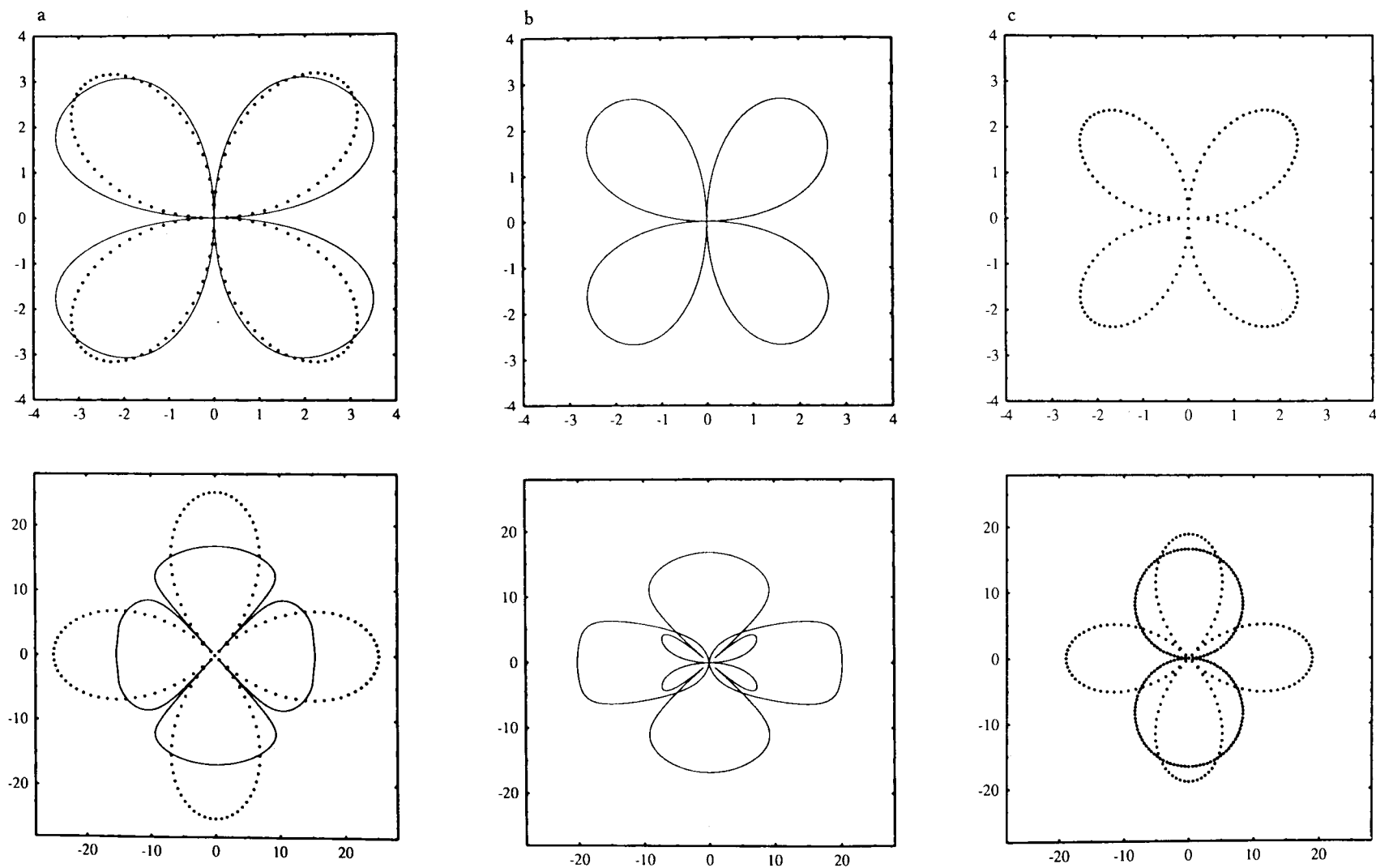


Figure 14. Theoretical radiation patterns of far-field high-frequency (top) quasi-compressional and (bottom) quasi-shear waves excited by a DC in an anisotropic medium intended to model the upper mantle (peridotite with systematically oriented olivine crystals) [after *Gajewski, 1993*]. The principal moment axes trend east-west and plunge at $\pm 45^\circ$. The a axes of the olivine crystals are oriented horizontally east-west. Dotted lines show radiation patterns in an isotropic medium, for comparison. (a) Amplitudes in an east-west vertical plane (the a - c plane of the olivine crystals). By symmetry, there is no quasi- SH wave in this case. (b) Amplitudes in a vertical plane striking 30° east of north. Two quasi-shear waves of intermediate polarization are excited. (c) Same as Figure 14b, for an isotropic medium. The two-lobed pattern is for horizontally polarized (SH) waves, and the four-lobed pattern is for waves polarized in the vertical plane of the figure (SV waves).

$$[\mathbf{A}^{+-1}\mathbf{A}^-]^T = \begin{bmatrix} 1 & 0 & 0 & 0 & 0 & R_1 \\ 0 & 1 & 0 & 0 & 0 & 0 \\ 0 & 0 & 1 & 0 & 0 & 0 \\ 0 & 0 & 0 & R_2 & 0 & 0 \\ 0 & 0 & 0 & 0 & R_2 & 0 \\ 0 & 0 & 0 & 0 & 0 & R_3 \end{bmatrix}, \quad (29)$$

where

$$R_1 \stackrel{\text{def}}{=} \frac{\lambda^- - \lambda^+}{\lambda^+ + 2\mu^+}, \quad (30)$$

$$R_2 \stackrel{\text{def}}{=} \frac{\mu^-}{\mu^+}, \quad (31)$$

$$R_3 \stackrel{\text{def}}{=} \frac{\lambda^- + 2\mu^-}{\lambda^+ + 2\mu^+}. \quad (32)$$

Figure 15 shows the distortion of the apparent mechanisms of DCs of various orientations occurring adjacent to a horizontal interface across which the elastic-wave speeds change by 20%. If the fault plane is parallel to the interface (or if the interface is the fault plane), then shear faulting does not lead to apparent non-DC mechanisms, although the scalar seismic moment is distorted. This case is not illustrated in the figure but is clear from the structure of the matrix in (29). Only M_{13} and M_{23} are nonzero, and matrix multiplication merely multiplies these elements by R_2 , producing a DC of the same orientation but with its moment multiplied by the ratio of the rigidity moduli. If the fault is perpendicular to the interface, then the apparent mechanism is still a DC for all slip directions, but its orientation and seismic moment are distorted, as the first column of the figure illustrates. For general fault orientations the apparent mechanism has artificial isotropic and CLVD components.

4.6. Rapid Polymorphic Phase Changes

Except in the shallowest parts of the crust, compressional stresses in the Earth greatly exceed shear stresses. Therefore earthquake processes that involve even relatively small volume changes could release large amounts of energy. For this reason it has long been speculated that polymorphic phase transformations in minerals might cause deep earthquakes. Such speculation has been stimulated also by consideration of the simple theory of frictional sliding, which seems to require impossibly large shear tractions when the confining pressure is high, and by the theory of plate tectonics, which involves large-scale vertical motions in the upper mantle. Many common minerals undergo polymorphic changes in crystal structure in response to changes in pressure and temperature, and some of the major structural features in the Earth, most notably the “transition region” at depths between about 400 and 800 km in the upper mantle, are attributed to such phase changes (in this case, involving the mineral olivine, $(\text{Fe, Mg})_2\text{SiO}_4$, trans-

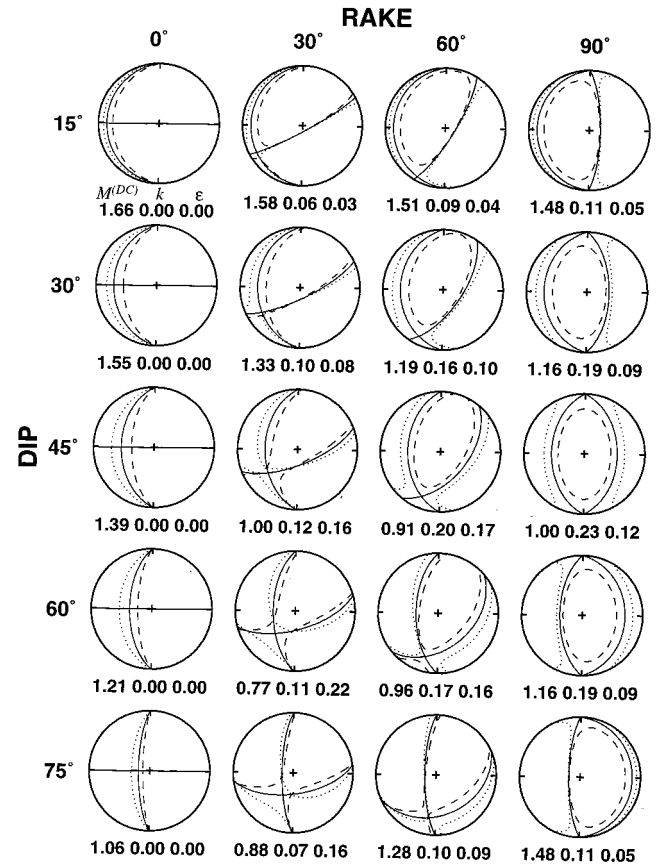


Figure 15. Apparent non-DC mechanisms caused by shear faulting with unit moment near a horizontal interface, for various dip and rake angles. Solid curves show compressional wave nodal planes corresponding to true (DC) mechanisms. Dotted curves show nodal surfaces for apparent mechanisms obtained if DC moment release on the low-speed side of interface is assumed to be on the high-speed side; dashed curves are the same, but with sides interchanged. Both media are Poisson solids, and the ratio of elastic moduli across the interface is 1.7:1, corresponding to a wave speed contrast of about 20% if density is proportional to wave speed. Numbers below each mechanism give the DC moment and the values of k and ϵ (equations (19) and (18)) corresponding to the dotted curves. Dips of 0 are not shown because the apparent mechanisms are DCs (although with moments distorted by the ratio of the rigidity moduli). Dips of 90° correspond to cases with rake of 0 (first column). Focal hemispheres (which may be considered either upper or lower) are shown in equal area projection.

forming to the spinel and then perovskite crystal structures).

As slabs of lithosphere subduct into the mantle, olivine and other minerals are carried out of their stability fields and into the stability fields of denser phases, into which they transform. If these changes occur rapidly enough to radiate seismic waves, they constitute earthquakes, and their mechanisms will have isotropic components. They probably will also have deviatoric components because the process of phase transformation will

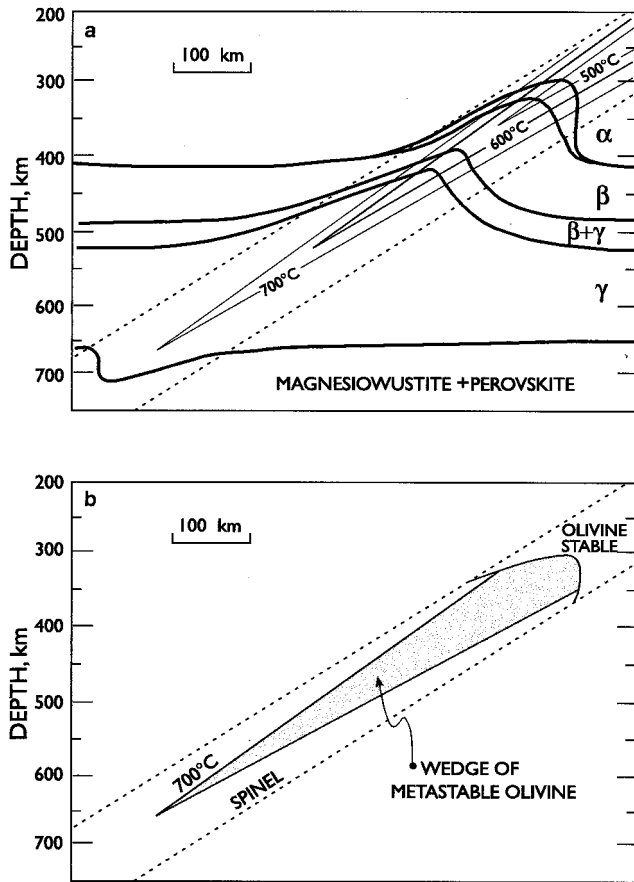


Figure 16. Transformational faulting mechanism for deep earthquakes. (a) schematic diagram of expected subduction zone temperature (thin lines) and olivine to spinel structure phase equilibrium (heavy lines). In equilibrium the $\alpha \rightarrow \beta$ and $\beta \rightarrow \gamma$ phase transformations occur at lower pressures for lower temperatures (transformations have positive Clapeyron slopes), so the phase boundaries are shallower within the subducting slab. (b) The transformational faulting model predicts that equilibrium will not be maintained at the lower temperatures near the middle of the subducting slab because of slower reaction rates. Thus a wedge of metastable olivine (α phase) (shaded) can exist within the slab, possibly as deep as 650 km. Transformational faulting earthquakes are predicted to occur when the metastable olivine transforms directly to spinel. The wedge narrows with depth, as the slab heats up, and the olivine \rightarrow spinel transformation takes place. Thus large deep earthquakes may occur on several adjacent short faults, rather than one long fault [Houston, 1993].

release shear strain, much as explosions are often observed to release tectonic shear strain [Toksöz and Keihner, 1972]. There seems to be no reason, however, why such a deviatoric component should be a DC rather than a CLVD, and in fact, the CLVD force system was first invented as a possible mechanism for deep earthquakes caused by phase transformations [Knopoff and Randall, 1970].

At least two effects can tend to inhibit rapid phase transformations. The first is thermal diffusion, which must occur to transfer the heat liberated or absorbed in

the transformation. The second is mass diffusion, which is needed to accommodate the chemical differentiation that accompanies many phase transformations such as those in solid solutions like olivine. Rather special conditions are probably required for a phase transformation to cause earthquakes.

In the laboratory, metastable minerals sometimes undergo rapid phase transformations within thin zones, which facilitate shear faulting and cause acoustic emissions, for example in ice [Kirby, 1987]. This “transformational-faulting” process might also occur in subduction zones in the Earth if, at the low temperatures within subducted slabs, olivine is carried to depths far outside its stability field (Figure 16) [Kirby et al., 1991]. The transformation of olivine directly to the spinel structure, bypassing the intermediate β spinel phase, is expected to be particularly efficient at radiating seismic waves. If the zones are thin enough, such a process could be consistent with observations that deep focus earthquakes have dominantly DC focal mechanisms, lacking significant isotropic components.

Transformational-faulting earthquakes are expected to have dominantly DC focal mechanisms, with small isotropic components whose magnitudes depend on the thicknesses of the zones of phase transformation. Resolving isotropic components in the presence of the distorting influences of near-source heterogeneity and anisotropy is a challenge for observational seismology.

The zone of metastable olivine is expected to become thinner with depth as the slab heats up and olivine transforms to the spinel structure (Figure 16). This narrowing would impose limits to the source dimensions of transformational earthquakes, and these limits would vary with depth and with fault orientation. Larger earthquakes would have to involve slip on multiple faults, and the non-DC components associated with such complex faulting (section 4.2) might produce a systematic increase in $|\epsilon|$ with magnitude and depth [Houston, 1993].

5. DISCUSSION

A wide variety of processes could cause earthquakes mechanisms to depart from the idealized double-couple force system that characterizes planar shear faulting in a homogeneous isotropic medium. These departures can be as extreme as unbalanced forces or torques, or they can be minor anomalies that are barely resolvable with the best data currently available.

Many of these processes, including unsteady fluid flow, shear faulting on ring structures, and tensile faulting (possibly combined with shear faulting) are particularly likely in geothermal and volcanic environments, where observed non-DC observations are commonest. A better understanding of these non-DC earthquakes may be useful in understanding and predicting volcanic activity and in prospecting for and exploiting geothermal energy.

Weak non-DC effects can result from departures from idealized models of shear faulting, such as fault complexity, dilatancy, fault-opening slip pulses, and heterogeneity and anisotropy of the host medium. Study of these effects will probably be valuable in refining our knowledge of how faults work. Such study will require improvements in our ability to resolve small non-DC components. Some current habits, such as constraining isotropic components of mechanisms to vanish and assuming temporal similarity between moment tensor components, hinder progress and should be discontinued.

ACKNOWLEDGMENTS. We thank S. Sipkin and H. M. Iyer for critically reviewing the manuscript and suggesting improvements. A. McGarr reviewed sections of the manuscript and made helpful suggestions. Dirk Gajewski provided valuable help in computing radiation patterns in anisotropic media. A portion of this research was supported by a G. K. Gilbert Fellowship from the U.S. Geological Survey and a Nuffield Foundation fellowship.

James A. Smith was the Editor responsible for this paper. He thanks Larry Ruff and two anonymous referees for their reviews.

REFERENCES

- Aki, K., Evolution of quantitative models of earthquakes, *SLAM AMS Proc.*, 12, 43–58, 1979.
- Aki, K., and P. G. Richards, *Quantitative Seismology: Theory and Methods*, 932 pp., W. H. Freeman, New York, 1980.
- Anderson, E. M., The dynamics of the formation of cone-sheets, ring-dykes, and cauldron-subsidences, *Proc. R. Soc. Edinburgh*, 56, 128–156, 1936.
- Anooshehpour, R., and J. N. Brune, Normal vibration, fault separation, and heat generation during stick-slip events in foam rubber, *Seismol. Res. Lett.*, 63, 75, 1992.
- Anooshehpour, R., and J. N. Brune, Frictional heat generation and seismic radiation in a foam rubber model of earthquakes, *Pure Appl. Geophys.*, 142, 735–747, 1994.
- Backus, G. E., Long-wave elastic anisotropy produced by horizontal layering, *J. Geophys. Res.*, 67, 4427–4440, 1962.
- Backus, G., Interpreting the seismic glut moments of total degree two or less, *Geophys. J. R. Astron. Soc.*, 51, 1–25, 1977.
- Backus, G., and M. Mulcahy, Moment tensors and other phenomenological descriptions of seismic sources, I, Continuous displacements, *Geophys. J. R. Astron. Soc.*, 46, 341–361, 1976a.
- Backus, G., and M. Mulcahy, Moment tensors and other phenomenological descriptions of seismic sources, II, Discontinuous displacements, *Geophys. J. R. Astron. Soc.*, 47, 301–329, 1976b.
- Brace, W. F., B. W. Paulding Jr., and C. H. Scholz, Dilatancy in the fracture of crystalline rocks, *J. Geophys. Res.*, 71, 3939–3953, 1966.
- Brune, J. N., S. Brown, and P. A. Johnson, Rupture mechanism and interface separation in foam rubber models of earthquakes: A possible solution to the heat flow paradox and the paradox of large overthrusts, *Tectonophysics*, 218, 59–67, 1993.
- Burridge, R., and L. Knopoff, Body force equivalents for seismic dislocations, *Bull. Seismol. Soc. Am.*, 54, 1875–1888, 1964.
- Chouet, B., Dynamics of a fluid-driven crack in three dimensions by the finite difference method, *J. Geophys. Res.*, 91, 13,967–13,992, 1986.
- Chouet, B., and B. R. Julian, Dynamics of an expanding fluid-filled crack, *J. Geophys. Res.*, 90, 11,187–11,198, 1985.
- Dahlen, F. A., Single-force representation of shallow landslide sources, *Bull. Seismol. Soc. Am.*, 83, 130–143, 1993.
- Dziewonski, A. M., and J. H. Woodhouse, Studies of the seismic source using normal-mode theory, in *Earthquakes: Observation, Theory and Interpretation*, edited by H. Kanamori and E. Boschi, pp. 45–137, North-Holland, New York, 1983.
- Dziewonski, A. M., T. A. Chou, and J. H. Woodhouse, Determination of earthquake source parameters from waveform data for studies of global and regional seismicity, *J. Geophys. Res.*, 86, 2825–2852, 1981.
- Dziewonski, A. M., G. Ekström, J. E. Franzen, and J. H. Woodhouse, Centroid-moment tensor solutions for January–March 1986, *Phys. Earth Planet. Inter.*, 45, 1–10, 1987.
- Ekström, G., Anomalous earthquakes on volcano ring-fault structures, *Eos Trans. AGU*, 75(16), Spring Meet. Suppl., 345, 1994.
- Eshelby, J. D., The determination of the elastic field of an ellipsoidal inclusion, and related problems, *Proc. R. Soc. London, Ser. A*, 241, 376–396, 1957.
- Fitch, T. J., D. W. McCowan, and M. W. Shields, Estimation of the seismic moment tensor from teleseismic body wave data with application to intraplate and mantle earthquakes, *J. Geophys. Res.*, 85, 3817–3828, 1980.
- Foulger, G. R., and R. E. Long, Anomalous local mechanisms: Tensile crack formation on an accreting plate boundary, *Nature*, 310, 43–45, 1984.
- Frohlich, C., The nature of deep focus earthquakes, *Annu. Rev. Earth Planet. Sci.*, 17, 227–254, 1989.
- Frohlich, C., Note concerning non-double-couple source components from slip along surfaces of revolution, *J. Geophys. Res.*, 95, 6861–6866, 1990.
- Frohlich, C., M. A. Riedesel, and K. D. Apperson, Note concerning possible mechanisms for non-double-couple earthquake sources, *Geophys. Res. Lett.*, 16, 523–526, 1989.
- Gajewski, D., Radiation from point sources in general anisotropic media, *Geophys. J. Int.*, 113, 299–317, 1993.
- Giardini, D., Systematic analysis of deep seismicity: 200 centroid-moment tensor solutions for earthquakes between 1977 and 1980, *Geophys. J. R. Astron. Soc.*, 77, 883–914, 1984.
- Gilbert, F., Excitation of the normal modes of the Earth by earthquake sources, *Geophys. J. R. Astron. Soc.*, 22, 223–226, 1970.
- Gilbert, G. K., A theory of the earthquakes of the Great Basin, with a practical application, *Am. J. Sci.*, 27, 49–54, 1884.
- Hart, R. S., Body wave studies of the September 20, 1969, North Atlantic Ridge earthquake (abstract), *Eos Trans. AGU*, 59, 1135, 1978.
- Hasegawa, H. S., and H. Kanamori, Source mechanism of the magnitude 7.2 Grand Banks earthquake of November 1929: Double couple or submarine landslide?, *Bull. Seismol. Soc. Am.*, 77, 1984–2004, 1987.
- Haskell, N. A., Total energy and energy spectral density of elastic wave radiation from propagating faults, *Bull. Seismol. Soc. Am.*, 54, 1811–1841, 1964.
- Hill, D. P., A model for earthquake swarms, *J. Geophys. Res.*, 82, 1347–1352, 1977.
- Houston, H., The non-double-couple component of deep earthquakes and the width of the seismogenic zone, *Geophys. Res. Lett.*, 20, 1687–1690, 1993.
- Hudson, J. A., R. G. Pearce, and R. M. Rogers, Source type plot for inversion of the moment tensor, *J. Geophys. Res.*, 94, 765–774, 1989.

- Isacks, B., J. Oliver, and L. R. Sykes, Seismology and the new global tectonics, *J. Geophys. Res.*, 73, 5855–5899, 1968.
- Ishimoto, M., Existence d'une source quadruple au foyer sismique d'après l'étude de la distribution des mouvements initiaux des secousses sismiques, *Bull. Earthquake Res. Inst. Univ. Tokyo*, 10, 449–471, 1932.
- Jost, M. L., and R. B. Hermann, A students guide to and review of moment tensors, *Seismol. Res. Lett.*, 60, 37–57, 1989.
- Julian, B. R., An inverse method for earthquake source mechanisms, *Tectonophysics*, 49, 223, 1978.
- Julian, B. R., Analysing seismic-source mechanisms by linear-programming methods, *Geophys. J. R. Astron. Soc.*, 84, 431–443, 1986.
- Julian, B. R., Volcanic tremor: Nonlinear excitation by fluid flow, *J. Geophys. Res.*, 99, 11,859–11,877, 1994.
- Julian, B. R., and G. R. Foulger, Earthquake mechanisms from linear-programming inversion of seismic-wave amplitude ratios, *Bull. Seismol. Soc. Am.*, 86, 972–980, 1996.
- Julian, B. R., and S. A. Sipkin, Earthquake processes in the Long Valley caldera area, California, *J. Geophys. Res.*, 90, 11,155–11,169, 1985.
- Kanamori, H., and J. W. Given, Analysis of long-period seismic waves excited by the May 18, 1980, eruption of Mount St. Helens: A terrestrial monopole?, *J. Geophys. Res.*, 87, 5422–5432, 1982.
- Kanamori, H., J. W. Given, and T. Lay, Analysis of seismic body waves excited by the Mount St. Helens eruption of May 18, 1980, *J. Geophys. Res.*, 89, 1856–1866, 1984.
- Kanamori, H., G. Ekström, A. Dziewonski, J. S. Barker, and S. A. Sipkin, Seismic radiation by magma injection: An anomalous seismic event near Tori Shima, Japan, *J. Geophys. Res.*, 98, 6511–6522, 1993.
- Kawakatsu, H., Centroid single force inversion of seismic waves generated by landslides, *J. Geophys. Res.*, 94, 12,363–12,374, 1989.
- Kawakatsu, H., Enigma of earthquakes at ridge-transform fault plate boundaries: Distribution of non-double couple parameter of Harvard CMT solutions, *Geophys. Res. Lett.*, 18, 1103–1106, 1991.
- Kawakatsu, H., Automated near-real-time CMT inversion, *Geophys. Res. Lett.*, 22, 2569–2572, 1995.
- Kawakatsu, H., K. Takano, S. Tsuboi, and Y. Yamanake, Automated pseudo-realtime CMT inversion (abstract), *Eos Trans. AGU*, 75(16), Spring Meet. Suppl., 234, 1994.
- Kawasaki, I., Azimuthally anisotropic model of the oceanic upper mantle, *Phys. Earth Planet. Inter.*, 43, 1–21, 1986.
- Kawasaki, I., and T. Tanimoto, Radiation patterns of body waves due to the seismic dislocation occurring in an anisotropic source medium, *Bull. Seismol. Soc. Am.*, 71, 37–50, 1981.
- Kirby, S. H., Localized polymorphic phase transformations in high-pressure faults and applications to the physical mechanism for deep earthquakes, *J. Geophys. Res.*, 92, 13,789–13,800, 1987.
- Kirby, S. H., W. B. Durham, and L. A. Stern, Mantle phase changes and deep earthquake faulting in subducting lithosphere, *Science*, 152, 216–225, 1991.
- Knopoff, L., and M. J. Randall, The compensated linear vector dipole: A possible mechanism for deep earthquakes, *J. Geophys. Res.*, 75, 4957–4963, 1970.
- Lachenbruch, A. H., and J. H. Sass, Heat flow and energetics of the San Andreas fault zone, *J. Geophys. Res.*, 85, 6185–6222, 1980.
- Langston, C. A., and D. V. Helmberger, A procedure for modeling shallow dislocation sources, *Geophys. J. R. Astron. Soc.*, 42, 117–130, 1975.
- Lawson, A. C., *The California Earthquake of April 18, 1906: Report of the State Earthquake Investigation Commission*, vol. I, 451 pp., Carnegie Inst. of Washington, Washington, D. C., 1908.
- Leary, P. C., S. Crampin, and T. V. McEvily, Seismic fracture anisotropy in the Earth's crust: An overview, *J. Geophys. Res.*, 95, 11,105–11,114, 1990.
- Maruyama, T., On the force equivalents of dynamic elastic dislocations with reference to the earthquake mechanism, *Bull. Earthquake Res. Inst. Univ. Tokyo*, 41, 467–486, 1963.
- McGarr, A., Moment tensors of ten Witwatersrand mine tremors, *Pure Appl. Geophys.*, 139, 781–800, 1992.
- Mendiguren, J. A., Inversion of surface wave data in source mechanism studies, *J. Geophys. Res.*, 82, 889–894, 1977.
- Miller, A. D., G. R. Foulger, and B. R. Julian, Non-double-couple earthquakes, 2, Observations, *Rev. Geophys.*, this issue.
- Mori, J., and C. McKee, Outward-dipping ring-fault structure at Rabaul caldera as shown by earthquake locations, *Science*, 235, 193–195, 1987.
- Okada, Y., Surface deformation due to shear and tensile faults in a half-space, *Bull. Seismol. Soc. Am.*, 75, 1135–1154, 1985.
- Okada, Y., Internal deformation due to shear and tensile faults in a half-space, *Bull. Seismol. Soc. Am.*, 82, 1018–1040, 1992.
- Pearce, R. G., and R. M. Rogers, Determination of earthquake moment tensors from teleseismic relative amplitude observations, *J. Geophys. Res.*, 94, 775–786, 1989.
- Price, N. J., *Fault and Joint Development in Brittle and Semi-brittle Rock*, 176 pp., Pergamon, New York, 1966.
- Reasenber, P., and D. Oppenheimer, FPFIT, FPLOT and FPPAGE: FORTRAN computer programs for calculating and displaying earthquake fault-plane solutions, *U.S. Geol. Surv. Open File Rep.*, 85-739, 1985.
- Reid, H. F., *The California Earthquake of April 18, 1906: Report of the State Earthquake Investigation Commission*, vol. II, *The Mechanics of the Earthquake*, 192 pp., Carnegie Inst. of Washington, Washington, D. C., 1910.
- Reidesel, M. A., and T. H. Jordan, Display and assessment of seismic moment tensors, *Bull. Seismol. Soc. Am.*, 79, 85–100, 1989.
- Sammis, C. G., and B. R. Julian, Fracture instabilities accompanying dike intrusion, *J. Geophys. Res.*, 92, 2597–2605, 1987.
- Savage, J. C., Radiation from a realistic model of faulting, *Bull. Seismol. Soc. Am.*, 56, 577–592, 1966.
- Scholz, C. H., *The Mechanics of Earthquakes and Faulting*, 439 pp., Cambridge Univ. Press, New York, 1990.
- Shimizu, H., S. Ueki, and J. Koyama, A tensile-shear crack model for the mechanism of volcanic earthquakes, *Tectonophysics*, 144, 287–300, 1987.
- Sipkin, S. A., Estimation of earthquake source parameters by the inversion of waveform data: Synthetic waveforms, *Phys. Earth Planet. Inter.*, 30, 242–259, 1982.
- Sipkin, S. A., Interpretation of non-double couple earthquake mechanisms derived from moment tensor inversion, *J. Geophys. Res.*, 91, 531–547, 1986.
- Sipkin, S. A., Rapid determination of global moment-tensor solutions, *Geophys. Res. Lett.*, 21, 1667–1670, 1994.
- Solomon, S. C., and B. R. Julian, Seismic constraints on ocean-ridge mantle structure: Anomalous fault-plane solutions from first motions, *Geophys. J. R. Astron. Soc.*, 38, 265–285, 1974.
- Stump, B. W., and L. R. Johnson, The determination of source properties by the linear inversion of seismograms, *Bull. Seismol. Soc. Am.*, 67, 1489–1502, 1977.
- Stump, B. W., and L. R. Johnson, Higher-degree moment tensors—The importance of source finiteness and rupture propagation on seismograms, *Geophys. J. R. Astron. Soc.*, 69, 721–743, 1982.
- Sykes, L. R., Mechanism of earthquakes and nature of faulting

- on the mid-oceanic ridges, *J. Geophys. Res.*, *72*, 2131–2153, 1967.
- Sykes, L. R., Focal mechanism solutions for earthquakes along the world rift system, *Bull. Seismol. Soc. Am.*, *60*, 1749–1752, 1970.
- Takei, Y., and M. Kumazawa, Why have the single force and torque been excluded from seismic source models?, *Geophys. J. Int.*, *118*, 20–30, 1994.
- Toksöz, M. N., and H. K. Kehrer, Tectonic strain release by underground nuclear explosions and its effect on seismic discrimination, *Geophys. J. R. Astron. Soc.*, *31*, 141–161, 1972.
- Ukawa, M., and M. Ohtake, A monochromatic earthquake suggesting deep-seated magmatic activity beneath the Izu-Oshima volcano, Japan, *J. Geophys. Res.*, *92*, 12,649–12,663, 1987.
- Urhammer, R., Broadband near-field moment tensor inversion (abstract), *Eos Trans. AGU*, *73*(43), Fall Meeting Suppl., 375, 1992.
- Voight, B., H. Glicken, R. J. Janda, and P. M. Douglass, Catastrophic rockslide avalanche of May 18, in *The 1980 Eruptions of Mt. St. Helens, Washington*, edited by P. W. Lipman and D. R. Mullineaux, *U.S. Geol. Surv. Prof. Pap.*, *1250*, 347–377, 1981.
- Wallace, T., A Re-examination of the moment tensor solutions of the 1980 Mammoth Lakes earthquakes, *J. Geophys. Res.*, *90*, 11,171–11,176, 1985.
- Woodhouse, J. H., The excitation of long period seismic waves by a source spanning a structural discontinuity, *Geophys. Res. Lett.*, *8*, 1129–1131, 1981.
- Zoback, M. D., et al., New evidence on the state of stress of San Andreas fault system, *Science*, *238*, 1105–1111, 1987.
-
- G. R. Foulger and A. D. Miller, Department of Geological Sciences, University of Durham, Durham, DH1 3LE, England, U.K.
- B. R. Julian, U.S. Geological Survey, 345 Middlefield Road, MS 977, Menlo Park, CA 94025. (e-mail: julian@andreas.wr.usgs.gov)

